The origin of iron silicides in ureilite meteorites

Aidan J. Ross[1,2], Hilary Downes[1,2,3,4]*, Jason S. Herrin[5†]

David W. Mittlefehldt[6], Munir Humayun[7], Caroline Smith[2]

[1]UCL/Birkbeck Centre for Planetary Sciences, University College London, Gower St, London, WC1E 6BT, UK

[2]Dept. of Earth Sciences, Natural History Museum, Cromwell Rd, London, SW7 5BD, UK

[3]Dept. of Earth and Planetary Sciences, Birkbeck University of London, Malet St., London, WC1E 7HX, UK

[4]Lunar and Planetary Institute/USRA, 3600 Bay Area Blvd, Houston, TX 77058, USA

[5] Earth Observatory of Singapore & Facility for Analysis, Characterisation, Testing, and Simulation, Nanyang Technological University, Singapore 639798

[6]Astromaterials Research Office, NASA Johnson Space Center, 2101 NASA Parkway, Houston, TX 77058, USA

[7]Department of Earth, Ocean and Atmospheric Science & National High Magnetic Field Laboratory, Florida State University, 1800 E. Paul Dirac Drive, Tallahassee, FL 32310, USA

†Previously at: ESC Astromaterials Research Group, Johnson Space Center, 2101 NASA Parkway, Houston, TX 77058, USA

*Corresponding Author.

3 Tables

11 Figures

Version of 12 September 2019

Keywords: Ureilites, Achondrites, Meteorites, Silicides, Metals

ABSTRACT

Ureilite meteorites contain iron silicide minerals including suessite $(Fe,Ni)_3Si$, hapkeite (Fe_2Si) and xifengite (Fe_5Si_3). Despite occurring mostly in brecciated varieties presumed to be derived from the regolith of the ureilite parent asteroid, suessite has also been confirmed in one lithology of a dimict ureilite (NWA 1241). In contrast, Si-bearing Fe-metals occur in both brecciated and unbrecciated ureilites, implying that they were formed throughout the ureilite parent asteroid. We examined major, minor and trace element data of Fe-metals in seven brecciated ureilites (DaG 319, DaG 999, DaG 1000, DaG 1023, DaG 1047, EET 83309, and EET 87720) in addition to the dimict ureilite NWA 1241.

In this study we show that the silicides and Si-bearing metals in ureilites have similar siderophile trace element patterns; therefore, the precursors to the silicides were indigenous to the ureilite parent body. Si-free kamacite grains in brecciated ureilites show flatter, more chondritic siderophile element patterns. They may also be derived from the interior of the ureilite parent body, but some may be of exogenous origin (impactor debris), as are rare taenite grains.

On Earth, iron silicides are often formed under high-temperature and strongly reducing conditions (e.g. blast furnaces, lightning strikes). On the Moon, hapkeite (Fe_2Si) and other silicides have been found in the regolith where they were formed by impact-induced space weathering. In the Stardust aerogel, iron silicides derived from comet Wild2 were also formed by an impact-related reduction process. Silicides in ureilite regolith breccias may have formed by similar processes but ureilites additionally contain abundant elemental carbon which probably acted as a reducing agent, thus larger and more abundant silicide grains were formed than in the lunar regolith or cometary material. The origin of suessite in NWA 1241 may be analogous to that of reduced lithologies in the terrestrial mantle, although a regolith origin may also be possible since this sample is shown here to be a dimict breccia.

1. INTRODUCTION

In 1982, Keil et al. discovered the first naturally occurring iron silicide in the brecciated ureilite meteorite North Haig. Ureilite meteorites are carbon-bearing ultramafic achondrites, most of which are unbrecciated and thought to represent samples of an asteroidal mantle (e.g. Scott et al., 1993; Goodrich et al., 2004). Their major and bulk trace element compositions are consistent with a restitic origin from a differentiated asteroid after loss of basaltic and metallic melts (e.g. Warren & Kallemeyn 1992; Mittlefehldt et al., 1998; Singletary & Grove 2003; 2006; Kita et al., 2004; Rankenburg et al., 2008). Some ureilites are polymict fragmental breccias consisting of welded lithic clasts and isolated mineral fragments (Jacques and

Fitzgerald, 1982; Prinz et al., 1987; Goodrich et al., 2004; Downes et al., 2008). Most clasts consist of typical ureilitic material but other materials are also found, including clasts similar to R- and E-chondrite types (Downes et al., 2008) and ureilitic melt rocks (Cohen et al., 2004). Solar wind implanted gases in some brecciated ureilites confirm a regolith origin (Ott et al., 1990, 1993, Rai et al., 2003).

The formation of ureilites is still a controversial and unsettled problem in meteoritics (e.g., Goodrich et al., 2007; 2013a; Warren, 2012). Nevertheless, the history of ureilite meteorites can be divided into two main stages (Warren and Kallemeyn 1989; Downes et al., 2008; Herrin et al., 2010). The original ureilite parent body had a range of initial silicate compositions (e.g., Warren, 2012) and experienced extensive partial melting of the metal-sulfide and silicate systems. Results from short-lived isotopic chronometers indicate that this differentiation occurred within ~1 Myr of formation of CAIs in the solar nebula (van Kooten et al., 2017). While it was still hot, the ureilite parent body experienced profound mechanical disruption by a large impact (Warren and Kallemeyn 1989; Herrin et al., 2010). Lithic fragments from disrupted portions of the ureilite parent body then reassembled to form a macroscopically brecciated daughter body around which a regolith formed and from which all ureilite meteorites appear to be derived. The Almahata Sitta meteorites derived from the fall of ~4 m diameter asteroid 2008 TC_3 in Sudan (Jenniskens et al., 2009) show that O-, E- and C chondrite fragments are common within the portion of the ureilite-dominated polymict breccia represented by this bolide (Goodrich et al., 2015).

Naturally occurring iron silicide minerals, first described and named by Keil et al. (1982), have been reported from many brecciated (polymict) ureilite meteorites (Mittlefehldt et al., 2007; Herrin et al., 2008; Smith et al., 2008; 2010; Ross et al., 2010), and from NWA 1241, originally described as being unbrecciated (Ikeda 2007). In contrast, Si-bearing metals occur in both brecciated and unbrecciated ureilites (Goodrich et al., 2013b), although some of them may be exogenic (Boleaga and Goodrich, 2019). We have investigated the nature, composition and origin of iron silicides and Si-bearing metals in several ureilites, in an attempt to determine their mode of formation Possibilities include that they could represent fragments of the core of the ureilite parent body (Ross et al., 2009), could have formed from reduction of silicate minerals in the mantle of the parent body (Keil et al., 1982), or formed by space weathering processes in the regolith similar to those which occur on the Moon (Anand et al., 2004).

We examined the petrography, major, minor and trace element chemistry of metal phases in eight ureilite samples: Dar al Gani (DaG) 319, DaG 999, DaG 1000, DaG 1023, DaG 1047, Elephant Moraine (EET) 83309, EET 87720, and northwest Africa (NWA) 1241. The first seven are brecciated ureilites, while NWA 1241 had previously been described as unbrecciated (Ikeda 2007) but we find it to be dimict. Most of these samples are well characterised for their silicate mineralogy (Downes et al., 2008). The EET samples are

known to be regolith-derived from studies of their noble gases (Ott et al., 1991, 1993). Some of the DaG might be paired, but this is difficult to determine for polymict breccias (cf., Goodrich et al., 2004).

2. BACKGROUND TO IRON SILICIDES AND SI-BEARING METALS

Fig. 1 shows the compositions of named iron silicide minerals as defined by the International Mineralogical Association (IMA). Keil et al. (1982) first described suessite from polymict ureilites and proposed that it formed within the ureilite mantle from reduction of silicates. Further ureilite silicides not analysed in this paper include hapkeite (Fe_2Si) in a section of dimict ureilite FRO 90228 reported by Smith (2008), and the presence of suessite, hapkeite and naquite in polymict ureilite DaG 1066 reported by Moggi Cecchi et al. (2015). Potentially extra-terrestrial iron silicides reported from cosmic dusts from the Yanshan mountains contain xifengite (Fe_5Si_3) and gupeiite (Fe_3Si) (Yu 1984), and deposits at the Younger Dryas boundary contain suessite ($(Fe,Ni)_3Si$) (Wu et al., 2013). Hapkeite is also an extremely rare phase in lunar regolith material (Anand et al., 2004) which may have an impact-induced vapor deposition origin. Other iron silicides, including FeSi and $FeSi_2$, have been found in lunar meteorite Dhofar 280 (Anand et al., 2004; Nazarov et al., 2012). Suttle and Genge (2017) found suessite in micrometeorites from Late Cretaceous chalks from the United Kingdom. Various iron silicides were found by Reitmeijer et al. (2008) in impact-produced aerogel tracks in samples from comet Wild2. Other extraterrestrial silicides such as perryite $(Ni,Fe)_8(Si,P)_3$ occur in the Horse Creek ungrouped iron meteorite (Buchwald 1975) and enstatite chondrites (Wasson and Wai 1970), whereas brownleeite (MnSi) is known from interplanetary dust (Nakamura-Messenger et al., 2010). Ni-rich silicides have recently been discovered in aubrite meteorites (Garvie et al., 2018). Silicides have not yet been reported from enstatite chondrite meteorites.

The Earth's mantle provides some rare examples of iron silicides. Several IMA-approved iron silicide minerals were originally found and described from the Luobusha ophiolite complex in Tibet (Fig. 1) where podiform mantle chromitites have yielded luobusaite ($Fe_{0.84}Si_2$; Bai et al., 2006), naquite (formerly known as fersilicite; FeSi; Shi et al., 2012) and linzhiite (formerly known as ferdisilicite: $FeSi_2$; Li et al., 2012). However, Ballhaus et al (2017) have suggested that these phases may have formed via lightning strikes on surface outcrops. Ishimaru et al. (2009) described iron-titanium silicides in mantle peridotite xenoliths from beneath Kamchatka (Russia), whereas Pankov and Spetsius (1989) and Shiryaev et al. (2008) reported the presence of $FeSi_2$ in mantle-derived kimberlites in Russia. Griffin et al. (2016) described Fe_3Si from mantle-derived materials in Late Cretaceous ash deposits on Mount Carmel in Israel, although a recent paper argues

that these and other mantle-derived super-reduced phases including the silicides may be caused by contamination during sample preparation (Litasov et al., 2019). Mavlyanovite (Mn_5Si_3), the manganese analogue of xifengite, has also been reported from a lamproite in Uzbekistan (Yusupov et al., 2009).

Fulgurites (rocks formed when lightening is discharged into the ground) are another source of naturally-occurring terrestrial iron silicides (e.g. Essene and Fisher 1986; Parnell et al., 2008). Pasek et al. (2012) reported the presence of Fe_3Si, Fe_2Si and Fe_5Si_3 (and possibly Fe_8Si_3 and Fe_7Si_3) in fulgurites from Pennsylvania. Silicides formed in fulgurites have experienced high temperatures and very low (atmospheric) pressures over a very short time span (e.g., Pasek and Pasek, 2018). Ballhaus et al (2017) produced xifengite in experiments in which basalt was exposed to artificial lightning strikes which formed high-temperature plasmas in the presence of graphite.

Artificial iron silicides are also formed at high temperatures and low pressures in industrial processes such as coke-making (Ye et al., 2013) and steel production (Viswanathan et al., 2009). Fig. 2 is part of a metallurgical phase diagram of the Ni-free Fe-Si at 1 atm pressure (Yuan et al., 2007), showing that the stable phases under these conditions are Fe_3Si (gupeiite), Fe_5Si_3 (xifengite) and FeSi (naquite).

Metals with up to 4 wt% Si occur in enstatite chondrite meteorites (Zhang et al., 1995) and up to 2.4 wt% Si in aubrites (Garvie et al., 2018). Lauretta et al. (2001) reported that metal in Type I chondrules contained up to 3.2 wt% Si. Fe,Ni metals in unbrecciated ureilites contain a maximum of 5 wt% Si (Goodrich et al., 2013b; Horstmann et al., 2014a). This leads to several questions concerning the relationship between the silicides in the asteroidal regolith and the indigenous Si-bearing metals in the asteroidal interior and whether conditions in the regolith environment might have favored iron silicide production.

3. ANALYTICAL METHODS

All samples were prepared or provided as polished sections. Initial examination was conducted, using petrographic microscopy and a scanning electron microscope (SEM). The SEM was used to obtain backscattered electron (BSE) images and for semi-quantitative energy dispersive spectroscopy to get an overview of sample textures, location of metallic minerals, and levels of oxidation caused by weathering. This information was used in preparation for analysis using the electron microprobe (EMPA) and laser-ablation inductively coupled plasma mass spectrometry (LA-ICP-MS) as described below.

Petrographic investigationsof EET 83309, EET 87720, DaG 319 and DaG 1047 were conducted on the JEOL 5900LV and LEO 1455VP SEMs at the Natural History Museum, London, with an accelerating voltage of either 15 kV or 20 kV and a beam current of ~2 nA.

All quantitative major and minor element analyses were done by electron microprobes using wavelength-dispersive spectroscopy. Compositions of metal and silicide phases in most samples were initially characterized at NASA Johnson Space Center on a Cameca SX100 microprobe. Typical operating parameters were a 20 kV accelerating voltage and a beam current of 40 nA. Standards for calibration were a combination of natural and synthetic minerals and metals. For larger grains, multiple analyses were performed to discern any compositional heterogeneity. Later analyses on silicides in NWA 1241 were performed using NASA's JEOL JXA 8530-F Field Emission electron microprobe. These analyses were done with an accelerating voltage of 15 kV, a 40 nA bean current, and the beam in spot mode (~0.3 μm) to achieve a finer resolution analysis volume for zoning profiles. For sample DaG 999 only, additional data on metals and silicides were obtained at Nanyang Technological University. Two new sections were studied using a JEOL JXA 8530-F Field Emission electron microprobe with an accelerating voltage of 15 kV and a 20 nA beam current. For samples DaG 319 and DaG 1047, electron microprobe data were collected on the Cameca SX100 instrument at the Natural History Museum, London, with an accelerating voltage of 20 kV and a beam current of 20 nA. Results are presented in Tables 1 (metals) and 2 (silicides).

Trace element concentrations for DaG 1000, EET 83309, EET 87720, and NWA1241 were determined at the Plasma Analytical Facility of the National High Magnetic Field Laboratory at Florida State University. Measurements were performed using a New Wave Research UP-213 (Nd:YAG 213 nm) laser ablation system coupled to a Finnigan Element™ magnetic sector ICP-MS. All analyses were performed using a laser repetition rate of 10 Hz and at 50% power output. Further information about the instrumentation setup used in this study, including typical relative sensitivity factors for analysis of metals, are detailed in Humayun et al. (2007). All data was acquired in low resolution mode ($m/\Delta m = 300$). Overall spot sizes varied from 30 to 150 μm, with most analyses performed at 30-40 μm. Because of the small grain sizes, certain elements (e.g. W, Mo) were below detection limit in many analyses and are not considered in our discussion. External calibration standards used were the IVB iron meteorite Hoba, the IIA iron meteorite North Chile (Filomena) and NIST SRM 1263a steel, chosen because of their well-determined element compositions from multiple analyses (Campbell and Humayun 1998; Campbell and Humayun 1999; Campbell et al., 2002; Wasson et al., 1989). Blank-corrected intensities were converted to elemental abundances by normalization to Ni content determined by previous EMP analyses. Analytical precision for most elements was <10% based on repeat measurements of calibration standards.

For DaG 319 and DaG 1047, trace elements were analyzed by LA-ICP-MS at NASA JSC using a New Wave UP-193 solid state laser ablation system attached to a Thermo Scientific Element XR™ magnetic sector ICP-MS in low resolution mode ($m/\Delta m = 300$). Laser power was 1-2 GW/cm^2, with a repetition rate of 10 Hz. Spot sizes varied from 20 to 100 μm, depending on metal/silicide grain size. External calibration standards used were the IVB iron meteorite Hoba, the IIA iron meteorite North Chile (Filomena), and NIST SRM 1168 and NIST SRM 1178 steels, chosen because of their well-determined element compositions from multiple analyses (Campbell and Humayun 1999; Campbell et al., 2002; Campbell and Humayun 2005; Wasson et al. 1989; Wasson et al. 1998). Corrected intensities were converted to elemental abundances by normalization to Ni content determined by previous EMP analyses. Where multiple isotopes were analyzed, a weighted mean was calculated.

4. PETROGRAPHY

Sections of eight meteorites were studied petrographically**.** These samples can be grouped into three sets: two cold desert samples from the Elephant Moraine area of Antarctica (EET 83309 and EET 87720), five hot desert samples from the Dar al Gani area of Libya (DaG 319, DaG 999, DaG 1000, DaG 1023 and DaG 1047), and one hot desert sample from Northwest Africa from a non-specific location in Libya (NWA 1241).

Seven of the samples have been previously classified as polymict, brecciated ureilites. EET 83309 and EET 87720 are similar in texture (Downes et al., 2008), although they are not paired. EET 83309 (Prinz et al., 1987) consists of angular clasts of ureilitic olivine, pigeonite and rare augite. EET 87720 similarly largely consists of clasts of shocked and unshocked ureilitic silicate minerals, in a brecciated matrix of similar material. Silicate minerals analysed by EMPA in several of the same meteorite sections were reported by Downes et al. (2008), where additional petrographic descriptions of these samples can also be found. All these clasts are within the normal range of silicate minerals from unbrecciated ureilites. Polymict ureilites DaG 319, DaG 999, DaG 1000, DaG 1023 and DaG 1047 have been described as coming from close proximity in the Dar al Gani area (Grossman, 1998; Russell et al., 2003; Connolly et al., 2007) but it is not known if they are actually paired. The DaG samples are similar in texture, containing numerous ureilitic silicate minerals of the range of compositions seen in unbrecciated ureilites, displaying different shock levels, as well as rare clasts of non-ureilitic material (e.g. Ikeda et al., 2000; Kita et al., 2004, Downes et al., 2008). Metals in the clasts of non-ureilitic material in EET 83309, EET 87720 and the DaG samples

(Downes et al., 2008; Ross et al, 2010) were excluded from this present study, as they are clearly unrelated to ureilites.

NWA 1241 was described as a monomict ureilite by Ikeda (2007), who stated that it was not brecciated and that it contained suessite. Until that discovery, suessite had only been described from polymict ureilites. We confirm the presence of suessite in this sample but have evidence for a dimict character of NWA 1241 (Fig. 3). We purchased a sample of NWA 1241 that consisted of two chips; a larger one that is coarse-grained with minimal evidence for alteration (hereafter, lithology A), and a smaller one that is finer-grained and heavily rusted (lithology B). Petrographic examination of thin-sections made from the two fragments confirmed that they are different lithologies and contain distinct textures and differing silicate compositions. The distinct petrography of NWA 1241-A and NWA 1241-B indicates that the original meteorite was certainly dimict and could have been polymict, contradicting the initial classification as a monomict ureilite based on a single thin section (Ikeda, 2007). Dimict ureilite meteorites consisting of two contrasting fragments of ureilites with different textures and mineral chemistry have previously been reported from the Frontier Mountains (FRO) area of the Antarctic by Smith et al (2000).

Based on mineral compositions and textures, lithology B is equivalent to the section described by Ikeda (2007). The texture of lithology B is difficult to ascertain because metallic phases in the chip are highly oxidized, which caused substantial expansion of intergranular boundaries, extensive dark staining (optical)/brightness (backscattered electrons), and facilitated substantial grain plucking (Fig. 3). Furthermore, thick reduced rims on olivine containing minute metal grains make their margins opaque, and these blend into the rusty regions where many of the Fe-silicides reside. Backscattered electron images suggest that lithology B might include intergranular brecciation, but this could be a weathering artifact in which expansion of metallic phases as they oxidized caused fragmentation of silicates. Regardless, lithology B is not a fragmental breccia. We analyzed 11 olivine cores in lithology B and their forsterite contents (Fo) have a narrow range of 82.2-83.0 (Fig. 4). We have analyzed 6 pyroxene cores and most of them have compositions of $Wo_{8.8}En_{76.4}Fs_{14.8}$, but one grain is more magnesian - $Wo_{8.4}En_{80.5}Fs_{11.1}$ (Fig. 4). Our analyses of lithology B phases match those of Ikeda (2007) (Fig. 4). Ikeda (2007) found suessite in his section of NWA 1241, and we have found it only in lithology B. In contrast, lithology A is metal-poor and has the typical ureilite granulitic texture consisting of coarse anhedral olivine and pyroxene grains that meet in triple junctions and have curved intergranular boundaries. Olivine cores in lithology A are uniform in composition with Fo of 89.1 ± 0.1 (Fig. 4). Pyroxene grains are pigeonite, with average core compositions of $Wo_{6.85\pm0.02}En_{83.56\pm0.04}Fs_{9.59\pm0.03}$ (Fig. 4).

Most of the silicides found in this study were suessite ($(Fe,Ni)_3Si$). We found xifengite (Fe_5Si_3) only in DaG 999 and EET 87720, and hapkeite was not observed in any of our samples. Iron silicides are observed in three distinct petrographic occurrences in ureilites:

a) "Interstitial" coarse suessite found in lithology B of NWA 1241 (Ikeda 2007; Mittlefehldt et al., 2007). This occurrence in the unbrecciated lithology B may allow for definition of the formation mechanism of silicide minerals within ureilites in general. The occurrence described in North Haig (Keil et al., 1982) appears to be similar. Fig. 5 shows examples of coarse in-situ suessite grains in NWA 1241-B. One grain occurs interstitial to four pyroxene grains in textural equilibrium and is texturally similar to grain boundary metal in unbrecciated ureilites (cf., Goodrich et al., 2013b). This homogeneous and abundant population of silicides may be close their site of production.
b) Fragments on the mm-µm-scale grains, found in EET 83309, EET 87720, DaG 319, DaG 1000, and DaG 1047 as isolated clasts or adhering to mineral or lithic fragments and are sometimes rounded. One grain in DaG 999 (Fig. 6) consists of two silicides of contrasting compositions, the larger portion being xifengite and the smaller part being suessite. The boundary between the two parts is sharp but not straight. Unfortunately, this grain was discovered too late to be included in the LA-ICP-MS study. Fig. 7 shows examples of silicides in EET 83309 and EET 87720, together with examples of kamacite, all of which have been analyzed by LA-ICP-MS. These silicides coexist with unrelated metals and sulfides (Herrin et al., 2006). This population was probably gardened from their original site of production and re-deposited in regolith breccias by impact.
c) Grains in "shock-melt veins" as described by Smith et al. (2008) in paired dimict ureilites FRO 90168/90228/93008 together with kamacite and iron phosphides. This is a disequilibrium assemblage wherein silicides were either stabilized locally at µm scales or else transported by shock melts. This observation may be significant in terms of the origin of ureilitic silicides.

5. COMPOSITIONS OF METALS AND SILICIDES

*5.1 EMP*A *results*

Tables 1 and 2 give major and minor element compositions for representative metal and silicides analyzed in the ureilite samples. Fig. 8 shows the variation in Ni and Si in all the individual analyses in different metal and silicide species, compared with metals in unbrecciated ureilites (Goodrich et al., 2013b; Horstmann et al., 2014a) and slightly greater than the highest amount of Si found in metals in enstatite chondrites (Zhang et al., 1995) and Type I chondrules (Lauretta et al., 2001). We have identified three types

of metal (Table 1): Si-free kamacite, Si-bearing kamacite, and taenite, as well as three types of silicide (Table 2): suessite, xifengite, and a third, non-stoichiometric type that we refer to as "low-Si silicides". Fig. 9a shows these defined phases on a ternary diagram of Fe–Si–Ni+Co and Fig. 9b shows their Ni-Co relationships. Fig. 2 shows a histogram for the number of grains of different Si contents found in this study.

We define Si-free kamacite here as containing ≤0.1 wt% Si and ≤6.91 wt% Ni (the maximum found in Si-free grain boundary metal in unbrecciated ureilites (Goodrich et al., 2013b)). Si-free kamacite is particularly abundant in a single large, mosaicised ureilitic clast in EET 87720, but also occurs in DaG 1047 and rarely (one grain per section) in samples DaG 319, DaG 1000, EET 83309 and NWA 1241-A. It contains 0.34-6.89 wt% Ni, 0.06-0.61 wt% Co, ≤0.33 wt% Cr and ≤1.53 wt% P.

Si-bearing kamacite grains are defined as those that plot within the field of grain boundary metal from unbrecciated ureilites reported by Goodrich et al. (2013b) and Horstmann et al. (2014a) to have 0.1 to 5.1 wt% Si and <8 wt% Ni (shown in the background of Fig. 8) We found Si-bearing kamacite in samples EET 83309, DaG 319, DaG 999, DaG 1000 and DaG 1047. They contain 0.13-4.91 wt% Si, 0.42-7.97 wt% Ni, 0.06-0.61 wt% Co, ≤1.3wt% Cr and 0.06-2.38 wt% P**.** The most Ni-rich of these have Ni contents outside the kamacite field in the Fe-Ni system (Yang et al., 1996), but the stability field for kamacite (α iron) expands to higher Ni contents with increasing Si and P contents (Ackerbauer et al., 2009).

Grains of taenite (classified here with Ni > 8 wt%), were found in EET 87720, DaG 999, DaG 1000 and DaG 1047. They show a wide range of Ni (up to 29 wt%) but low Si contents (mostly below detection limit). It is likely that they are derived from chondritic impactors in the same way that some of the silicate minerals in brecciated polymict ureilites are derived (Downes et al., 2008), since taenite has never been reported in grain boundary metal from unbrecciated ureilites. As such, trace element data for these metals are not considered and we do not discuss their origin further.

Table 2 reports representative major and minor element compositions of the ureilitic silicides. Fig. 8 shows a detailed inset for the mineral suessite. Found mostly in NWA 1241-B and DaG 1023 but present in all samples except NWA 1241-A, it has a distribution maximum near stoichiometric suessite: $(Fe,Ni)_3Si$ (Fig. 2) but with a range of Ni contents (Fig. 8). Keil et al. (1982) also found a range of compositions that they defined as suessite (outlined in the inset of Fig. 8) with a low-Ni and high-Ni divide at 2.7 wt%. Keil et al. (1982) found that low-Ni suessite dominated their sample, whereas here high-Ni suessite is the dominant phase in almost all samples where suessite is found. The range of Ni values here does not exceed the 6.4 wt% found by Keil et al. (1982), we found a maximum of 5.65 wt%, but the minimum Ni was found to be 0.08 wt%, lower than the 0.5 wt% found by Keil et al. (1982). Such low Ni content could be considered to

be gupeiite, although this grain contains more Si than the ideal gupeiite. Keil et al. (1982) gave atomic proportions for two averaged suessites: low-Ni suessite $(Fe,Ni,Co,Cr)_{\sum=2.84}(Si,P)_{\sum=1}$ and high-Ni suessite $(Fe,Ni,Co,Cr)_{\sum=3.14}(Si,P)_{\sum=1}$. Here we define suessite using atomic proportions with the full range from $(Fe,Ni,Co,Cr)_{\sum=2.52}(Si,P)_{\sum=1}$ to $(Fe,Ni,Co,Cr)_{\sum=3.46}(Si,P)_{\sum=1}$. This corresponds to a Si range of 12.48-16.79 wt% (expanded from that of Keil et al. (1982) of 12.6-16.4 wt%). The suessite also contains 0.06-0.43 wt% Co, 0.05-1.46 wt% Cr and ≤0.64 wt% P.

Three grains with compositions close to xifengite (Fe_5Si_3) were found, with 1.01-3.91 wt% Ni, 0.1-0.3 wt% Co, 0.89-1.29 wt% Cr and 0.28-0.81 wt% P (Table 2). A microprobe traverse across a DaG 999 grain, which consists of two phases in contact, shows that Ni, Cr and P all increase across the boundary from suessite to xifengite (Fig. 6). Mn was also higher in the xifengite part of the grain than in the suessite (Fig. 6b). The Cr content is variable within the xifengite, with distinctly higher values in the center of the grain.

An intermediate group with Si contents between the Si-bearing kamacite and suessite has a wide range of non-stoichiometric Si contents (Fig. 2) and we classify these as "low-Si silicides" (Fig. 8 and Fig. 9a). These grains have Si contents between 5.13 and 12.2 wt % and have Ni between 0.07 and 7.6 wt%. These compositions have not been reported by previous studies of ureilite metals or silicides (Keil et al., 1982; Goodrich et al., 2013b; Horstmann et al., 2014a). Minor element concentrations are 0.06-0.47 wt% Co, ≤1.11 wt% Cr and ≤0.79 wt% P. The apparent continuous range of Si contents between the grain boundary metal compositions of Goodrich et al. (2013b) and the suessite compositions may indicate either very fine-scale mixtures of silicide and metal, or the presence of metal alloys with variable Si contents.

A strong positive correlation is observed between Co and Ni in the metals and silicides (Fig. 9b). There is no clear distinction between any of the defined metal and silicides groups and our data overlap the range of those from Goodrich et al. (2013b) for grain boundary metals in unbrecciated ureilites. Goodrich et al. (2013b) found a non-chondritic Ni/Co ratio of 13.6 in metals from unbrecciated ureilites. Our data fall close to the same trendline and trendlines through the groups of each metal and silicide type fall close to or on the trendline defined by Goodrich et al. (2013b). The fact that most of the Si-free kamacite data have non-chondritic Ni/Co ratios implies that these minerals were not derived from chondritic impactors but are part of the suite of indigenous ureilitic metals. The lunar hapkeite analysis (Anand et al., 2004) clearly falls away from the ureilitic data, and plots below the chondritic ratio.

5.2 LA-ICP-MS results

Table 3 contains siderophile trace element data for metal and silicide phases. Results are displayed in Fig. 10, normalized to Ni and to chondritic abundances (Lodders, 2003).

Si-free kamacite was analyzed in two samples: DaG 1047 and EET 87720. The latter have near-chondritic patterns or else are depleted in only the most compatible siderophiles (Fig. 10a). Despite their flat patterns, the Si-free kamacites may still be indigenous to the ureilite parent body, as Goodrich et al. (2013b) found similar flat patterns in metals in the unbrecciated ureilite ALHA 81101, which is also a highly shocked ureilite similar to the lithology where these grains were found. Si-free kamacites in DaG 1047 are individual grains scattered in the sample and not associated with any particular lithology, but all fall within the ranges of the data found in grain boundary metals from unbrecciated ureilites by Goodrich et al. (2013b), given as background data in Fig. 10a. Most of the DaG 1047 Si-free kamacite grains have enrichments in the compatible siderophile elements relative to EET 87720 Si-free kamacite grains, but have very similar incompatible siderophile element contents.

Si-bearing kamacite was analyzed in DaG 310, DaG 1000, DaG 1047 and EET 83309, as shown in Fig. 10b. All grains plot within the field for grain boundary metal from unbrecciated ureilites, with the exception of lower Ge values for many of the analyses. One grain in DaG 1047 has a close to flat pattern and could have originated from a Si-bearing metal grain from an E-chondrite clast, but still falls within the ureilitic grain boundary field.

Siderophile element patterns of silicides are variable between grains (Fig. 10c and 10d). Most are fractionated, with the highly compatible siderophile elements (Re-Pt) enriched relative to incompatible siderophile elements (Pd, Au) in a manner similar to that observed in bulk ureilites (Warren et al., 2006; Rankenburg et al., 2008) and in individual grains of many grain boundary metals in ureilites (Goodrich et al., 2013b). Siderophile trace element patterns in bulk unbrecciated ureilites are highly fractionated as a legacy of extensive extraction of metallic sulfide partial melts (Warren et al., 2006; Rankenburg et al., 2008). The metals in unbrecciated ureilites usually show strong siderophile element fractionation (Goodrich et al., 2013b), and because they host the majority of siderophile elements, it is not surprising that bulk ureilites show this pattern. Ureilitic silicides have this same fractionation pattern. There is no significant difference between the fractionation patterns for suessite and xifengite, or between silicides and the Si-bearing kamacite, nor correlation with the Si content of the grains (Fig. 11a). The most meaningful difference between the silicides and grain boundary metals is the Ga/Ge ratio (Fig. 11b); here Ga/Ge>1 for almost all silicides whereas Ga/Ge<1 for most grain boundary metal in unbrecciated ureilites (Goodrich et al. 2013b).

6. DISCUSSION

In this section, we evaluate the evidence for primary and/or secondary formation of Fe-silicides in ureilites. Three explanations could be proposed for the origin of the silicides:

1) They are exogenic to the ureilite parent body and were incorporated into ureilite regolith breccia samples by impact or were injected into lithologies such as NWA 1241-B;

2) Silicides formed within the ureilite parent body in lithologies such as NWA 1241-B that have since been incorporated into the breccias. This would imply that samples like NWA 1241-B are underrepresented in our collections of unbrecciated ureilites;

3) The silicides formed by a reducing process in the regolith of the ureilite source body and were injected into lithologies such as NWA 1241 as a Fe-Si melt.

We have demonstrated that regolith breccia ureilites contain a variety of metals and silicides (Figs. 8 and 9). We have shown that suessite-bearing NWA 1241 is a dimict breccia (Fig. 3 and 4), contrary to previous work which examined only one thin-section that contained a single lithologic component of the rock (Ikeda, 2007). Silicides have not been reported in any other monomict or unbrecciated ureilites and their occurrence thus appears to be restricted to brecciated samples and one lithology of NWA 1241. Because textures in our sample of NWA 1241-B are obscured by terrestrial alteration, we cannot claim that intergranular brecciation is entirely absent. However, Ikeda (2007) stated that the suessite-bearing section of NWA 1241 he studied was unbrecciated. Regardless, we have demonstrated that the silicides in NWA 1241-B are in textural equilibrium with the silicates, and not in breccia contact (Fig. 5). Silicides are not in chemical equilibrium with surrounding Fe-silicates and thus appear either to have formed within the regolith (for polymict breccias), or to have been included in ureilites by some physical process such as injection of Fe-Si melts. The texture of NWA 1241-B and siderophile trace element compositions of silicides indicate they are indigenous to the ureilite parent body, and Ikeda (2007) concluded that silicides in polymict ureilites were incorporated into the regolith by admixture of a NWA 1241-like lithology.

The fact that extra-terrestrial Fe-silicides occur mostly in regolith breccia ureilites and are also found in the lunar regolith could imply that some process acting on the surfaces of airless bodies may have been responsible for their formation. The high temperatures (1230-1100ºC) and extreme reducing conditions necessary for silicide formation (Ikeda 2007) could not have acted on the ureilite asteroidal regolith for long, as they would have quickly homogenized much of the mineralogical and textural diversity observed. Iron silicides can only be in equilibrium with FeO-bearing ureilite silicates at very low oxygen fugacities, so the process that produced them may have required the presence of carbon which is common in ureilites.

Additional evidence for short-duration, non-equilibrium processing of metal in ureilites is provided by the presence of nucleosynthetic Os isotope heterogeneity, including in DaG 319 (Goderis et al., 2015), one of the samples studied here.

The partial melting which left ureilites as residues involved removal of metal-sulfide and basaltic silicate fractions (Warren and Huber 2006). While ureilites typically contain low abundances of metal and sulfide in comparison to other types of achondrites such as HEDs, concentrations of highly refractory/compatible siderophile elements are sometimes present at greater than chondritic abundances in the bulk rocks (Rankenburg et al., 2008). This observation is consistent with the hypothesis that significant fractions of incompatible material have been removed from the parental asteroid, resulting in passive concentration of the more compatible components. The remaining metallic fraction in a typical ureilite is enriched in elements which are most compatible in the solid phase during metal-sulfide melting relative to incompatible elements (Rankenburg et al., 2008; Goodrich et al., 2013b).

Many of the Si-rich kamacites and silicides from the ureilites studied here have the high compatible/incompatible signature typical of bulk unbrecciated and monomict ureilites. Therefore, their trace element composition was likely inherited from Si-bearing metals formed as restites during melting in the metal-sulfide system within the ureilite parent body. This is consistent with the textural occurrence of suessite, mostly as fragments, but also as coarse interstitial grains in NWA 1241-B. Individual grains tend to be homogeneous in major and trace element but different grains have different compositions within the same sample. The difference in Ga/Ge ratios between the silicides and grain boundary metals (Goodrich et al., 2013b) is plausibly due to the silicides having undergone a more significant level of reduction, since Ga could be reduced from surrounding silicates (Schmitt et al., 1989). The similarity in overall fractionation pattern, in combination with the high T, low-fO_2 conditions required for suessite formation (Ikeda, 2007), indicates that the silicides may have been derived from Si-bearing metals within the ureilite parent body.

The Si-rich kamacites could have been the source of the siderophile elements found in the silicides, but the source of the additional Si in the silicides is not so clear. Hapkeite in the lunar regolith was considered by Anand et al. (2004) to have been formed by either reduction by solar wind or condensation from vapor. If the silicides formed on the ureilite parent asteroid, this combination of high-T and low-P could only be realized in the near-surface of a carbon-rich source during or shortly after impact, and therefore was mainly experienced by regolith material. The observation that iron silicides were formed by impacts onto Stardust aerogel (Rietmeijer et al., 2008) also suggests a very short-duration, high-temperature event.

However, suessite grains in NWA 1241-B do not display textural evidence for *in-situ* formation by a very rapid, high-T process. The suessite is interstitial between four pyroxene grains, and the grains are either included within pyroxene or at grain boundaries (Fig. 5). These textures are compatible with suessite having formed in, or been mobilized into, the interstices of the silicate framework. The example grains shown in Fig. 5 are in C-poor areas (C would be black in these images). The pyroxene in Fig. 5a shows very minimal reduction (slightly darker blue color) whereas that in Fig. 5b shows more extensive evidence for reduction, and the olivine has reduced rims (lighter green). However, the metal grains in these reduced rims are barely resolved (micron/sub-micron-sized) while the suessite grains are tens of microns in size. Thus, our results on NWA 1241-B do not support an *in-situ* reduction process for formation of suessite in the presence of FeO-bearing pyroxene and olivine for this case, but rather a more persistent process at greater depth within the fractured crust of the parent body.

One scenario that might explain the results on NWA 1241-B and the trace element data on silicides is that the silicides were part of a reduced assemblage that accreted late to the parent body. However, although enstatite chondrites form part of the assemblage of foreign fragments in polymict ureilites (including Almahata Sitta), there are also abundant fragments of much more oxidized material, none of which contain silicides. None of the enstatite chondrite fragments analysed so far contain silicides but many of them contain metal with up to 5.6 wt% Si (Horstmann et al.,2014b). However, their siderophile trace element patterns are chondritic, unlike those found in silicides in ureilites. A second scenario is that silicide in NWA 1241-B was formed as part of the high-T process that melted some of the reduced metals. Fractional melting in the metal-sulfide system allowed the early-formed, low-T melts to separate from the ureilitic restites, leaving behind restitic, compatible-siderophile-element-rich metal grains. If, during the melting process, the restite metal had been in equilibrium with a Fe-S-Si liquid, trace elements that are Si-avoiding would tend to concentrate in the low-Si metal, e.g. Ga, Ge, As and Au (Chabot et al., 2010). However, the siderophile element data for ureilitic silicides and grain boundary metal (kamacites) do not show different tendencies to concentrate the Si-avoiding elements defined by Chabot et al. (2010) (Fig. 10), as would be expected for this scenario. From this siderophile element evidence it is inferred that Si likely entered pre-existing metal grains under subsolidus, reducing conditions. The Fe-Si phase diagram (Fig. 2) shows that addition of Si to the system reduces the melting temperature. This suggests that the high-Si contents of compatible-siderophile-element-rich metals in ureilites were engendered by high-T reduction of the silicate phase, and that Si-rich metals were not part of the initial accretion assemblage to the ureilite parent body. However, this scenario does not provide a ready explanation for apparent lack of chemical reaction between Si-rich metal and FeO-bearing silicates, as documented in Fig. 5. Rapid injection of Fe-Si melts during

impact followed by fast cooling may be one explanation for the silicides in NWA 1241, particularly as this sample is now known to be dimict breccia and hence may have been close to the surface of the parent body.

7. CONCLUSIONS

A wide variety of metals and Fe-silicides in different petrographic contexts have been analyzed in a suite of polymict breccia ureilites, which probably represent the regolith of their parent body, and in the dimict ureilite NWA 1241. The metals are of three main types: Si-free kamacite which shows a range of Ni contents, Si-bearing kamacite, and taenite. Both Si-free and Si-bearing kamacites occur in unbrecciated ureilite grain boundary metal. Our major, minor and trace siderophile element results on metals closely resemble those reported from unbrecciated ureilites indicating that they were likely indigenous to the ureilite parent body. Taenite, however, has not been found in unbrecciated ureilites, and is therefore probably of impactor origin.

The silicides form three types: abundant suessite with variable Ni contents, rare xifengite, and a group of "low-Si silicide" grains that have Si contents between those of Si-bearing kamacite metals and stoichiometric suessites. In one case (DaG 999) a grain is composed of two distinct silicides (suessite and xifengite) in contact. Siderophile element patterns for the silicides are similar to those for the low-Si silicides and the Si-bearing kamacite, indicating a close relationship.

The silicides may have been derived from the Si-bearing kamacite by a process of reduction which occurred mainly in the regolith, similar to the impact-induced space weathering process on the Moon. However, suessite in NWA 1241-B appears to be in textural equilibrium with the ureilite silicates and may either have formed at greater depth within the ureilite parent body or was injected as a metallic melt. This sample has been shown in our study to be dimict and hence part of a breccia, which suggests that it may have been formed quite close to the surface of the parent body.

The different occurrences of natural silicides in terrestrial and extraterrestrial environments clearly indicate a variety of different origins. Silicides such as suessite and xifengite were mostly formed in situ on the ureilite parent asteroid perhaps by impacts that produced high T and (in the presence of abundant carbon) low fO_2. Thus, silicides in polymict ureilites were mostly formed by a short-lived, high temperature process that acted in the near-surface environment of their parent asteroid. This is a very different process from that which formed silicides in the terrestrial mantle, and more closely resembles that which formed Fe-silicides in the lunar regolith. The difference between the lunar and ureilite cases may be the result of the much

higher abundances of carbon in the latter. We cannot exclude a deeper origin (e.g. reduction in the asteroid mantle) for the suessite found in NWA 1241.

8. ACKNOWLEDGEMENTS

We would like to thank the reviewers F. Langenhorst and Anonymous for their comments and suggestions for improving this manuscript, and F. Langenhorst and A. Krot for handling this submission. We thank the ANSMET program and the U.S. Antarctic Meteorite Program for recovery and allocation of the Elephant Moraine ureilites examined as part of this study. This work was supported in part by grants from the NASA Cosmochemistry and Planetary Science Research Programs to DWM and MH. We acknowledge NERC funding for a CASE studentship with the NHM to AJR; and a Leverhulme Trust grant to HD. AJR would like to thank J. Spratt, A. Ball and A. Kearsley for analytical assistance at the NHM. The DaG and NWA 1241 samples were purchased from Erich Haiderer.

FIGURE CAPTIONS:

Fig. 1. Compositions of iron silicide minerals identified by IMA, including idealized compositions and actual compositions from which idealized compositions were derived. Composition of Earth's core from McDonough (2003)

Fig. 2. Fe-Si binary phase diagram at atmospheric pressure with ideal Fe-silicides phases up to 50 atomic % labelled (modified after Yuan et al., 2007). Histogram: atomic % Si for all grains in this study.

Fig. 3. Merged element maps and backscattered electron images of NWA 1241 lithologies A and B showing textural differences. Locations of textural details of suessite shown in Figs. 5 and 5b are indicated.

Fig. 4. Silicate mineral compositions for two lithologies of NWA 1241, compared with average data from Ikeda (2007).

Fig. 5. Merged element maps and backscattered electron images of examples of suessite in NWA 1241 lithology B. Different textural settings are: a. grain-boundary metal between pyroxene grains; b. suessite grains at juncture of olivine and pyroxene grains. Bright yellow areas in both images indicate high-Ni suessite.

Fig. 6. (a) BSE image and (b) false color Si map of a silicide grain in DaG 999, showing two phases (suessite and xifengite). EPMA data of the traverse indicated by the arrow across the boundary between suessite and xifengite in (a) are plotted in (c) for major elements and (d) for minor elements. Spikes in total weight % in (c) indicate bad data points.

Fig. 7. BSE images for metals and silicides in EET 83309 and EET 87720. Image (i) shows low-Si silicide from EET 83309; images (ii) and (iii) show suessite grains from EET 83309; image (iv) shows kamacite from EET 87720; image (v) shows xifengite from EET 87720; image (vi) shows kamacite with high Ni content from EET 87720.

Fig. 8. Si vs Ni in silicides and metals from brecciated ureilites from this work. Silicide compositions from Keil et al. (1982) (KK'82), Ikeda (2007), Anand et al. (2004) (MA'04), and ideal IMA compositions for gupeiite, hapkeite and xifengite are shown. Also shown as background data are those from literature grain boundary (GB) metals in unbrecciated ureilites from Goodrich et al. (2013b), Horstmann et al. (2014a), and Warren & Rubin (2010). Inset shows entire range of suessite compositions found by Keil et al. (1982). All silicides contain Ni within the range of ureilite grain boundary metal but more Si. Individual data points are plotted by meteorite analyzed.

Fig. 9. (a) Atomic % ternary diagram of Fe-Si-Ni+Co in silicides and metals from this study. Data points are plotted by mineral, as defined in Figure 8. Grey lines represent intervals of 10 atomic %, with the base cut off at 50 atomic % Fe. (b) Plot of Ni vs Co weight % in silicides and metals (excluding taenite). Data for grain boundary metals in unbrecciated ureilites are shown in the background for comparison, as well as their trend (Goodrich et al., 2013b).

Fig. 10. Chondrite-normalized siderophile element abundances for: (a) Si-free kamacite; (b) Si-bearing kamacite; (c) low-Si silicides; (d) suessite and xifengite.

Fig. 11. (a) Ir/Pd vs. Si weight % from EPMA analysis for different mineral types; (b) Ga/Ni vs Ge/Ni for different mineral types.

TABLE CAPTIONS

Table 1. Representative major element compositions of metals in brecciated ureilites and NWA 1241-B. bdl = below detection limit; na = not analysed.

Table 2. Representative major element compositions of silicides in brecciated ureilites and NWA 1241-B bdl = below detection limit; na = not analysed.

Table 3. Trace element compositions of silicides and metals in brecciated ureilites and NWA 1241-B. Ni (highlighted) was used for internal calibration. Where multiple spot sizes are given, this means the data was averaged from two analyses on the same grain. Si weight % from EPMA analysis. bdl = below detection limit (with detection limit given in brackets for LA-ICP-MS data).

REFERENCES

Ackerbauer S., Krendelsberger N., Weitzer F., Hiebl K. and Schuster J. C 2009. The constitution of the ternary system Fe–Ni–Si. *Intermetallics* 17, 414-420.

Anand M, Taylor L A, Nazarov M A, Shu J, Mao H-K and Hemley R J 2004. Space weathering on airless planetary bodies: clues from the lunar mineral hapkeite. *Proc. Nat. Acad. Sci.,*101, 6847-6851

Bai W, Shi N, Fang Q, Li G, Xiong M, Yang J and Rong H. 2006. Luobusaite, a new mineral. *Acta Geologica Sinica.* 80, 656-659.

Ballhaus C, Wirth R, Fonseca R O C, Blanchard H, Pröll W, Bragagni A, Nagel T, Schreiber A, Dittrich S, Thome V, Hezel D C, Below R and Cieszynski H. 2017. Ultra-high pressure and ultra-reduced minerals in ophiolites may form by lightning strikes. *Geochemical Perspectives Letters* 5, 42-46.

Berkley J. L. and Jones J. H. 1982. Primary igneous carbon in ureilites: Petrological implications. Proceedings, 13th Lunar and Planetary Science Conference, *Journal of Geophysical Research* 87(supplement): A353-A364.

Berkley J. L., Taylor G. J., Keil K., Harlow G., and Prinz M. 1980. The nature and origin of ureilites. *Geochimica et Cosmochimica Acta* 44:1579-1597.

Boleaga Y and Goodrich C A 2019. Xenolithic Fe,Ni metal in polymict ureilite meteorites. 50th LPSC Abstract # 1622.

Buchwald V F 1975. Handbook of iron meteorites. Volume 2, 661-664

Campbell A J and Humayun M 1998. Microanalysis of platinum group elements in iron meteorites using Laser Ablation ICP-MS. 30th LPSC Abstract # 1974

Campbell A J and Humayun M 1999. Trace element microanalysis in iron meteorites by Laser Ablation ICPMS. *Anal. Chem*. 71, 939-946

Campbell A J and Humayun M 2005. Compositions of group IVB iron meteorites and their parent melt. *Geochimica et Cosmochimica Acta* 69, 4733-4744.

Campbell A J, Humayun M and Weisberg M K 2002. Siderophile element constraints on the formation of metal in the metal-rich chondrites Bencubbin, Weatherford, and Gujba. *Geochimica et Cosmochimica Acta* 66, 647-660.

Chabot N L, Safko T M and McDonough W F 2010. Effect of silicon on trace element partitioning in iron-bearing metallic melts. *Meteoritics & Planetary Science* 45, 1243-1257.

Cohen B A, Goodrich C A and Keil K 2004 Feldspathic clast populations in polymict ureilites: Stalking the missing basalts from the ureilite parent body. *Geochimica et Cosmochimica Acta* 68, 4249-4266.

Connolly H C, Smith C, Benedix G, Folco L, Righter K, Zipfel J, Yamaguchi A, Chennaoui Aoudjehane H. 2007. The Meteoritical Bulletin #92. *Meteoritics & Planetary Science* 42, 1647-1694.

Downes H, Mittlefehldt D. W., Kita N. T., and Valley J.W. 2008. Evidence from polymict ureilite meteorites for a disrupted and re-accreted single ureilite parent asteroid gardened by several distinct impactors. *Geochimica et Cosmochimica Acta* 72:4825-4844.

Essene E J and Fisher D C 1986. Lightning strike fusion: extreme reduction and metal-silicate liquid immiscibility. *Science* 234, 198-193.

French B V and Eugster H P 1965. Experimental control of oxygen fugacities by graphite-gas equlibriums, *Journal of Geophysical Research* 70, 1529-1539.

Garvie L A J, Ray S, Wadhwa M, Wittman A and Domanik K 2018. Scrutinising six silicide-bearing samples of metal from the Norton County aubrite. 49th LPSC abstract # 2104.

Goderis S, Brandon A D, Mayer B and Humayun M 2015. S-process Os isotope enrichment in ureilites by planetary processing. *Earth Planetary Science Letters* 431, 110-118.

Goodrich C. A. and Berkley J. L. 1986. Primary magmatic carbon in ureilites: Evidence from cohenite-bearing metallic spherules. *Geochimica et Cosmochimica Acta* 50:681-691.

Goodrich C. A., Scott E. R. D., and Fioretti A. M. 2004. Ureilitic Breccias: Clues to the petrologic structure and impact disruption of the ureilite parent asteroid. *Chemie de Erde 64: 283-327.*

Goodrich C.A., Van Orman J.A. and Wilson L. 2007. Fractional melting and smelting on the ureilite parent body. *Geochimica et Cosmochimica Acta* 71, 2876-2895.

Goodrich C.A., Wilson L., Van Orman J.A. and Michel P. 2013a. Comment on "Parent body depth-pressure-temperature relationships and the style of the ureilite anatexis" by P. H. Warren (MAPS 47:209–227). *Meteoritics & Planetary Science* 48, 1096-1106.

Goodrich C A, Ash R D, Van Orman J A, Domanik K and McDonough W F 2013b. Metallic phases and siderophile elements in main group ureilites: Implications for ureilite petrogenesis. *Geochimica et Cosmochimica Acta* 112, 340-373.

Goodrich C A, Hartmann W K, O'Brien D P, Weidenschilling S J, Wilson L, Michel P and Jutzi M. 2015. Origin and history of ureilitic material in the solar system: The view from asteroid 2008TC3 and the Almahata Sitta meteorite. *Meteoritics and Planetary Science* 50, 782-809.

Griffin WL, Gain S E M, Adams D T, Huang J-X, Saunders M, Toledo V, Pearson N J and O'Reilly S Y 2016. First terrestrial occurrence of tistarite (Ti_2O_3): Ultra-low oxygen fugacity in the upper mantle beneath Mount Carmel, Israel. *Geology*, 44, 815-818.

Grossman J N. 1998. The Meteoritical Bulletin, No. 82, 1998 July. *Meteoritics and Planetary Science* 33, Supplement A221-A239.

Herrin J S, Mittlefehldt D W, Downes H and Humayun M 2008. Diverse metals and sulfides in polymict ureilites EET 83309 and EET 87720. 38th LPSC abstract # 2404

Herrin J S, Mittlefehldt D W and Jones J H 2008. Petrogenesis of Fe,Si metals in brecciated ureilites. 71st Annual Meteoritical Society Meeting Abstract # 5327

Horstmann M, Humayun M, Fisher-Gödde M, Bischoff A and Weybrauch M 2014a. Si-bearing metal and niningerite in Almahata Sitta fine-grained ureilites and insights into the diversity of metal on the ureilite parent body. *Meteoritics and Planetary Science* 49, 1948-1977.

Horstmann M, Humayun M, and Bischoff A 2014b. Clues to the origin of metal in Almahata Sitta EL and EH chondrites and implications for primitive E chondrite thermal histories. *Geochim. Cosmochim. Acta.* 140, 720-744.

Humayun M, Simon S B and Grossman L 2007. Tungsten and hafnium microdistribution in calcium-aluminum inclusions (CAIs) from Allende and Efremovka. *Geochim. Cosmochim. Acta* 71, 4609-4627.

Ikeda Y 2007. Petrology of an unusual ureilite NWA 1241. *Polar Science* 1, 45-53.

Ikeda Y, Prinz M, Nehru C. 2000. Lithic and mineral clasts in the Dar al Gani (DaG) 319 polymict ureilite. *Antarctic Meteorite Research* 13, 177-221.

Ishimaru S, Arai S, and Shukuno H 2009. Metal-saturated peridotite in the mantle wedge inferred from metal-bearing peridotite xenoliths from Avacha volcano, Kamchatka. *Earth Planet. Sci. Lett*. 284, 352-360.

Jenniskens P., Shaddad M., Numan D., Elsir S., Kadoda A., Zolensky M., Le L., Robinson G. A., Friedrich J., Rumble D., Steele A., Chesley S., Fitzsimmons A., Duddy S., Hsieh H., Ramsay G., Brown P., Edwards W., Tagliaferri E., Boslough M., Spalding R., Dantowitz R., Kozubal M., Pravec P., Borovicka J., Charvat Z., Vaubaillon J., Kuiper J., Albers J., Bishop L., Mancinelli R., Sandford S., Milam S., Nuevo M. and Worden S. 2009. The impact and recovery of asteroid 2008 TC_3. *Nature* 458:485-488.

Keil K, Berkley J L and Fuchs L H 1982, Suessite, Fe_3Si: a new mineral in the North Haig ureilite. *American Mineralogist* 67, 126-131

Kita N. T., Ikeda Y., Togashi S., Liu Y., Morishita Y. and Weisberg M. K. 2004. Origin of ureilites inferred from a SIMS oxygen isotopic and trace element study of clasts in the Dar al Gani 319 polymict ureilite. *Geochimica et Cosmochimica Acta* 68:4213-4235.

Lauretta D S, Buseck P R and Zega T J. 2001. Opaque minerals in the matrix of the Bishunpur (LL3.1) chondrite: constraints on the chondrule formation environment. *Geochimica et Cosmochimica Acta* 65, 1337-1353.

Li G, Bai W, Shi N, Fang Q, Xiong M, Yang J, Ma Z and Rong H 2002. Linzhiite, $FeSi_2$, a redefined and revalidated new mineral species from Luobusha, Tibet, China. *European Journal of Mineralogy*, 24, 1047-1052

Litasov K D, Kagi H and Bekker T B. 2019. Enigmatic super-reduced phases in corundum from natural rocks: Possible contamination from artificial abrasive materials or metallurgical slags. *Lithos* 340-341: 181-190.

Lodders K. 2003. Solar System Abundances and Condensation Temperatures of the Elements. *The Astrophysical Journal* 591, 1220-1247.

McDonough W F 2003, Compositional model of the Earth's core. In: Treatise on Geochemistry, volume 2, 547-568.

Mittlefehldt D. W., McCoy T. J., Goodrich C. A., and Kracher A. 1998. Non-chondritic meteorites from asteroidal bodies, In: *Planetary Materials, editor Papike J. J. Reviews in Mineralogy and Geochemistry 36. Mineralogical Society of America, Washington, DC, pp 4.1-4.195.*

Mittlefehldt D W, Herrin J S, and Downes H 2007. Petrology and geochemistry of new ureilites and ureilite genesis. 70th Meteoritical Society Meeting, Abstract #5280.

Moggi Cecchi V, Caporali S, and Pratesi G 2015. DaG 1066: A newfound anomalous ureilite with chondritic inclusions. 78th Annual Meeting of the Meteoritical Society. Abst. # 5252.

Nakamura-Messenger K, Keller L P, Clemett S J, Messenger S R, Jones J H, Palma R L, Pepin R O, Klock W, Zolensky M E and Tatsuoka H 2010. Brownleeite: a new manganese silicide mineral in an interplanetary dust particle. *American Mineralogist*, 95 221-228.

Nazarov M A, Demidova S I, Anosova M O, Kositsyn Yu A, Ntaflos Th and Brandstetter F 2012. Native silicon and iron silicides in the Dhofar 280 lunar meteorite. *Petrology* 20, 506-519.

Ott U., Löhr H. P., and Bergemann F. 1990. EET 83309: a ureilite with solar noble gases. *Meteoritics* 25, 396 (Abstract)

Ott U., Löhr H. P., and Bergemann F. 1993. Solar noble gases in polymict ureilites and an update on ureilite noble gas data. *Meteoritics 28:415-416.*

Pankov VYu and Spetsius Z V 1989. Inclusions of iron silicides and native silicon in moissanite from the Sytykanskaya kimberlite pipe. *Doklady Acad, Nauk*. SSSR 305, 152-155 (in Russian)

Parnell J, Thackrey S, Muirhead D, and Wright A 2008. Transient high-temperature processing of silicates in fulgurites as analogues for meteorite and impact melts. 39th LPSC, Abstract # 1286.

Pasek M. A. and Pasek V. D. 2018. The forensics of fulgurite formation. *Mineralogy Petrology* 112, 185–198. https://doi.org/10.1007/s00710-017-0527-x.

Pasek M A, Block K and Pasek V 2012. Fulgurite morphology: a classification scheme and clues to formation. *Contrib. Mineral. Petrol* 164, 477-492.

Prinz M., Weisberg M. K., Nehru C. E., and Delaney J. S. 1987. EET 83309, a polymict ureilite: recognition of a new group. *Lunar and Planetary Science* 18:802–803.

Rai V. K., Murthy A. V. S. and Ott U. 2003. Noble gases in ureilites: cosmogenic, radiogenic and trapped components. *Geochimica et Cosmochimica Acta* 67:4435–4456.

Rankenburg K., Humayun M., Brandon A. D., and Herrin J. S. 2008. Highly siderophile elements in ureilites. *Geochimica et Cosmochimica Acta* 72:4642-4659.

Reitmeijer F J M, Nakamura T, Tsuchiyama A, Uesugi K, Nakano T and Leroux H 2008. Origin and formation of iron silicide phases in the aerogel of the Stardust mission. *Meteoritics and Planetary Science* 43, 121-134.

Ross A J, Downes H, Smith C L and Jones A P 2009. Highly reduced metals and sulfides in ureilites: remnants of the UPB core? *Meteoritics and Planetary Science* 44, #5269 (Abst).

Ross A J, Downes H, Smith C L and Jones A P. 2010. DaG 1047: a polymict ureilite containing exotic clasts including a chondrite. 41st LPSC Abstract #2361.

Russell S S, Zipfel J, Grossman J N and Grady M M 2002. The Meteoritical Bulletin 86, 2002 July. *Meteoritics and Planetary Science* 37, Supplement A157-A184

Russell S S, Zipfel J, Falco L, Jones R, Grady M M, McCoy T and Grossman J N 2003. The Meteoritical Bulletin 87. *Meteoritics and Planetary Science* 38, Supplement A189-A248.

Schmitt W, Palme H and Wänke H 1989. Experimental determination of metal/silicate partition coefficients for P, Co, Ni, Cu, Ga, Ge, Mo, and W and some implications for the early evolution of the Earth. *Geochimica et Cosmochimica Acta* 53, 173-185

Scott E. R. D., Taylor J. G., and Keil K. 1993. Origin of ureilite meteorites and implications for planetary accretion. *Geophysical Research Letters 20:415-418.*

Shi N, Bai W, Li G, Xiong M, Yang J, Ma Z, Rong H 2012. Naquite, FeSi, a new mineral species from Luibusha, Tibet, Western China. *Acta Geologica Sinica* 86, 533-538.

Shiryaev A A, Griffin W L, Stoyanov E and Kagi H 2008. Natural silicon carbide from different geological settings: polytypes, trace elements, inclusions. 9th Int. Kimb. Conf. Extended Abst. 9IKC-A-00075.

Singletary S. J. and Grove T. L. 2003. Early petrogenetic processes on the ureilite parent body. *Meteoritics and Planetary Science* 38:95-108.

Singletary S. J. and Grove T. L. 2006. Experimental constraints on ureilite petrogenesis. *Geochimica et Cosmochimica Acta* 70, 1291-1308

Smith C L, Wright I P, Franchi I A and Grady M M 2000. A statistical analysis of mineralogical data from Frontier Mountains ureilites. *Meteoritics and Planetary Science* 35, #5, Supplement p A150.

Smith C L, Downes H, and Jones A P 2008. Metal and sulphide phases in interstitial veins in "dimict" ureilites – insights into the history and petrogenesis of the Ureilite Parent Body. 39th LPSC Abstract # 1669.

Smith C L, Ross A J, and Downes H 2010. Iron silicide in polymict ureilites – recording the complex history of the ureilite parent body. Abstract # 5221, 73rd Meeting of Meteoritical Society.

Suttle M D and Genge M J 2017. Diagenetically altered fossil micrometeorites suggest cosmic dust is common in the geological record. *Earth Planet. Sci. Lett*. 476, 132-142.

van Kooten E.M.M.E., Schiller M. and Bizzarro M. 2017. Magnesium and chromium isotope evidence for initial melting by radioactive decay of ^{26}Al and late stage impact-melting of the ureilite parent body. *Geochimica et Cosmochimica Acta* 208, 1-23.

Viswanathan A, Sastikumar D, Kumar H and Nath A K., 2009. Formation of WC-iron silicide (Fe_5Si_3) composite clad layer on AISI 316L stainless steel by high power (CO_2) laser. *Surface and Coatings Technology* 203, 1618-1623.

Warren P.H. 2012. Parent body depth–pressure–temperature relationships and the style of the ureilite anataxis. *Meteoritics & Planetary Science* 47, 209-227.

Warren P. H. and Kallemeyn G. W. 1989. Geochemistry of polymict ureilite EET 83309, and a partially disruptive impact model for ureilite origin. *Meteoritics* 24:233-246.

Warren P. H. and Kallemeyn G. W. 1992. Explosive volcanism and the graphite-oxygen fugacity buffer on the parent asteroid(s) of the ureilite meteorites. *Icarus* 100:110-126.

Warren P. H. and Huber H. 2006. Ureilite petrogenesis: A limited role for smelting during anatexis and catastrophic disruption. *Meteoritics and Planetary Science* 41:835-849.

Warren P H, Ullf-Moller F, Huber 2006. H and Kallemeyn G W 2006. Siderophile geochemistry of ureilites: a record of early stages of planetesimal core formation. *Geochimica et Cosmochimica Acta* 70, 2104-2126

Warren P H and Rubin A E. 2010. Pyroxene-selective impact smelting in ureilites. *Geochimica et Cosmochimica Acta* 74, 5109-5133.

Wasson J T and Wai C M 1970. Composition of the metal, schreibersite and perryite of enstatite achondrites and the origin of enstatite chondrites and achondrites. *Geochimica et Cosmochimica Acta* 34, 169-184

Wasson J T, Ouyang X, Wang J, and Jerde E. 1989. Chemical classification of iron meteorites: XI. Multi-element studies of 38 new irons and the high abundance of ungrouped irons from Antarctica. *Geochimica et Cosmochimica Acta* 53, 735-744.

Wasson J, Choi B-G, Jerde E, Ulff-Møller F. 1998. Chemical Classification of Iron Meteorites: XII. New Members of the Magmatic Groups. *Geochimica et Cosmochimica Acta*: 62, 715-724.

Wu Y, Sharma M, LeCompte M A, Vemitroff M N, and Landis J D 2013. Origin and provenance of spherules and magnetic grains at the Younger Dryas boundary. *Proc. Nat. Acad. Sci.,* 110, 3557-3566.

Yang C.-W., Williams D. B. and Goldstein J. I. 1996. A revision of the Fe-Ni phase diagram at low temperatures (<400 °C). *Journal of Phase Equilibria* 17, 522-531.

Ye Z, Gupta S, Kerkkonen O, Kanniala R, and Sahajwalla V., 2013. SiC and ferro-silicides formation in Tuyere cokes. *Iron and Steel Institute of Japan International* 53, 181-183.

Yu Z 1984. Two new minerals gupeiite and xifengite in cosmic dusts from Yanshan. *Acta Petrologica Mineralogica et Analytica*. 3, 231-238.

Yuan W J, Li R, Shen Q and Zhang L M., 2007. Characterization of the evaluation of the solid solubility of Si in sintered Fe-Si alloys using DSC technique. *Materials Characterization* 58, 376-379

Yusupov R G, Stanley C J, Welch M D, Spratt J, Cressey G, Rumsey M S, Seltmann R and Igamberdiev E 2009. Mavlyanovite, Mn_5Si_3: a new mineral species from a lamproite diatreme, Chatkal Ridge, Uzbekistan. *Mineralogical Magazine* 73, 43-50

Zhang Y, Benoit P and Sears D W 1995. The classification and complex thermal history of the enstatite chondrites. *Journal of Geophysical Research: Planets*, 100, 9417-9438.

Zolensky M. E., Herrin J. S., Mikouchi T., Ohsumi K., Friedrich J., Steele A., Fries M., Sanford S., Hagiya K., Takeda H., Colbert M., Hanna R., Maisano J., Ketcham R., Le L., Robinson G.-A., Jenniskens P., and Shaddad M. H. 2010. Mineralogy and Petrography of the Almahata Sitta Ureilite. *Meteoritics and Planetary Science.* 45, 1618-1637.

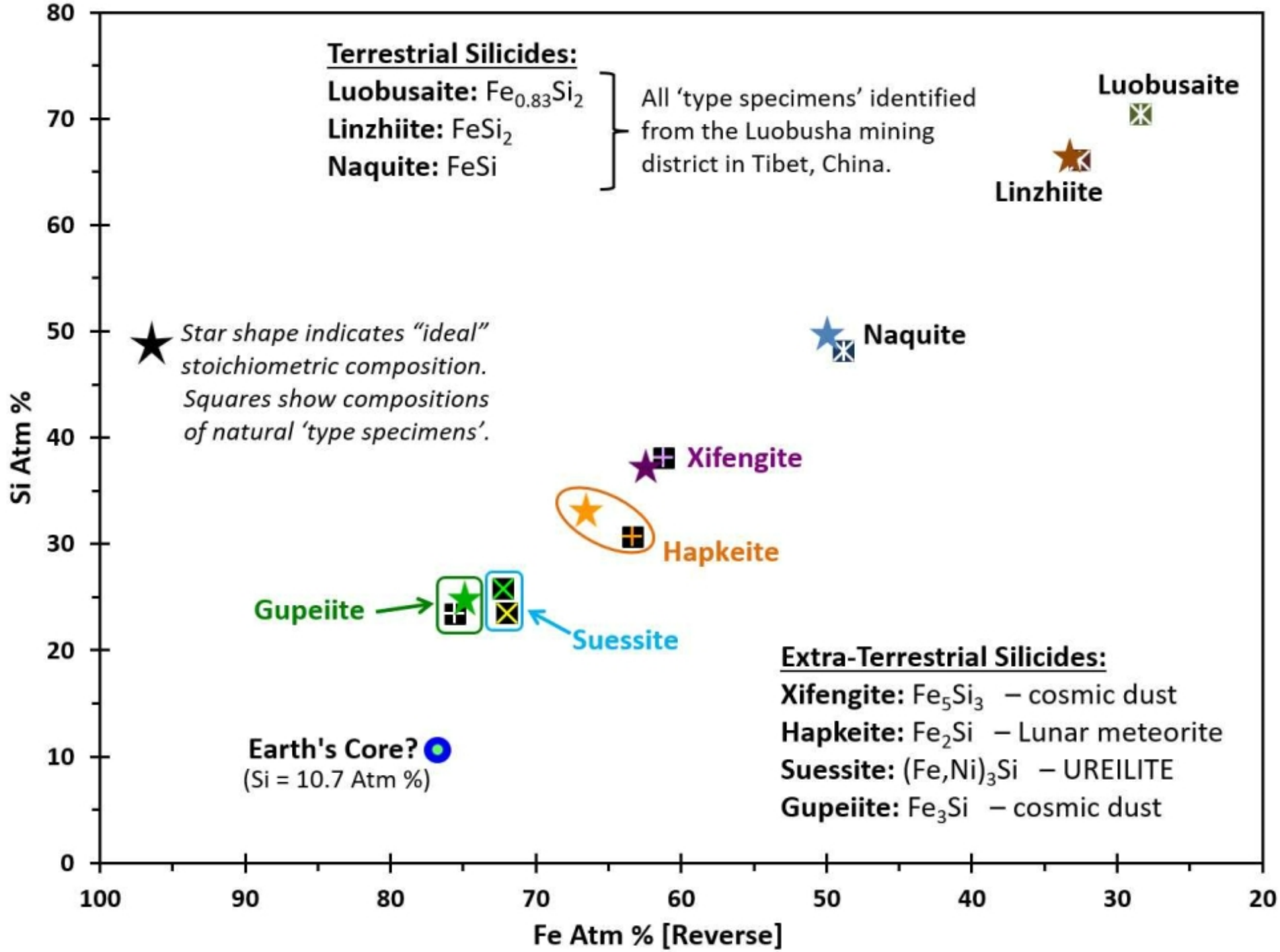
Terrestrial Silicides:
Luobusaite: $Fe_{0.83}Si_2$
Linzhiite: $FeSi_2$
Naquite: FeSi
All 'type specimens' identified from the Luobusha mining district in Tibet, China.
Luobusaite
Linzhiite
Star shape indicates "ideal" stoichiometric composition. Squares show compositions of natural 'type specimens'.
Naquite
Xifengite
Hapkeite
Gupeiite
Suessite
Earth's Core?
(Si = 10.7 Atm %)
Extra-Terrestrial Silicides:
Xifengite: Fe_5Si_3 – cosmic dust
Hapkeite: Fe_2Si – Lunar meteorite
Suessite: $(Fe,Ni)_3Si$ – UREILITE
Gupeiite: Fe_3Si – cosmic dust
Si Atm %
0
10
20
30
40
50
60
70
80
100
90
80
70
60
50
40
30
20
Fe Atm % [Reverse]

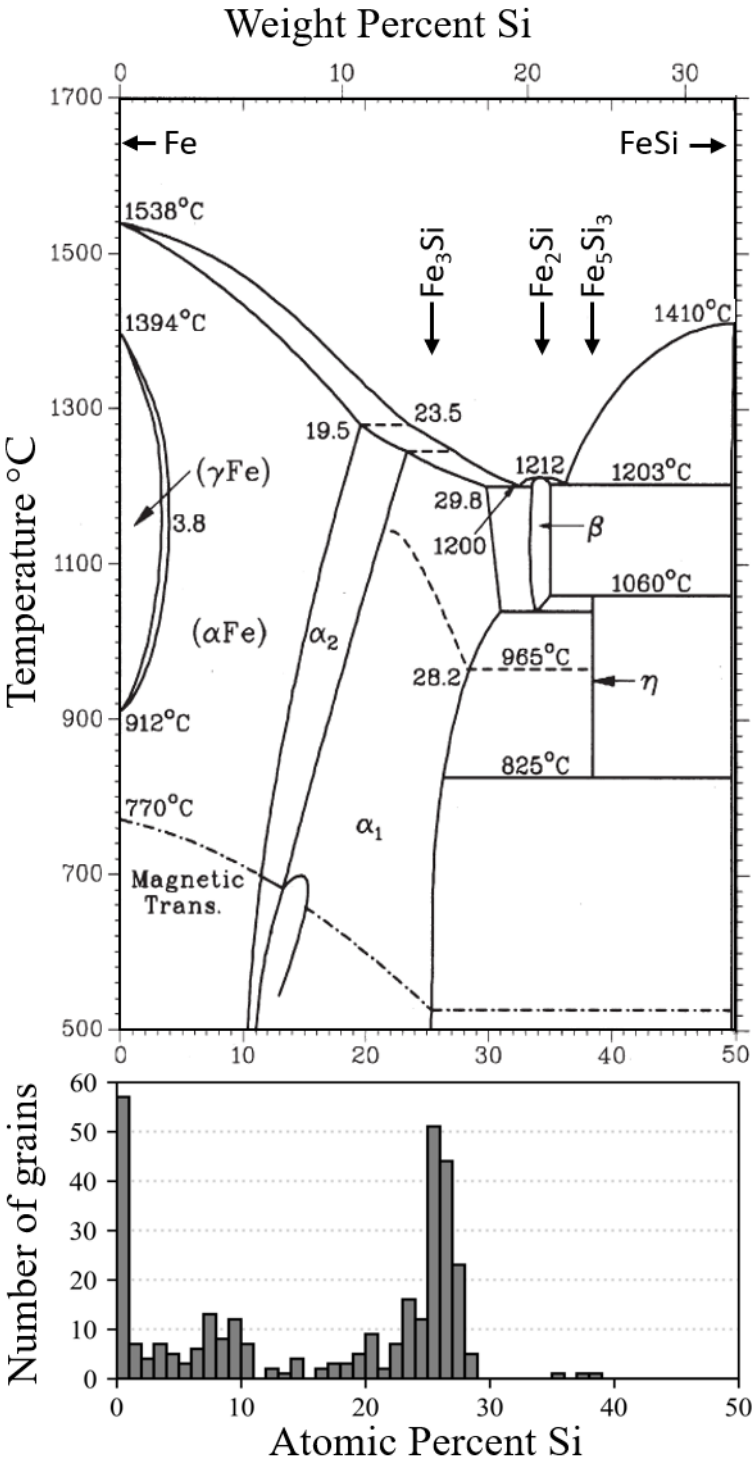
Weight Percent Si
Fe
FeSi
1538°C
1394°C
1410°C
Fe3Si
Fe2Si
Fe5Si3
23.5
19.5
1212
1203°C
29.8
1200
β
1060°C
(γFe)
3.8
(αFe)
α2
965°C
28.2
η
912°C
825°C
770°C
α1
Magnetic
Trans.
Temperature °C
Number of grains
Atomic Percent Si

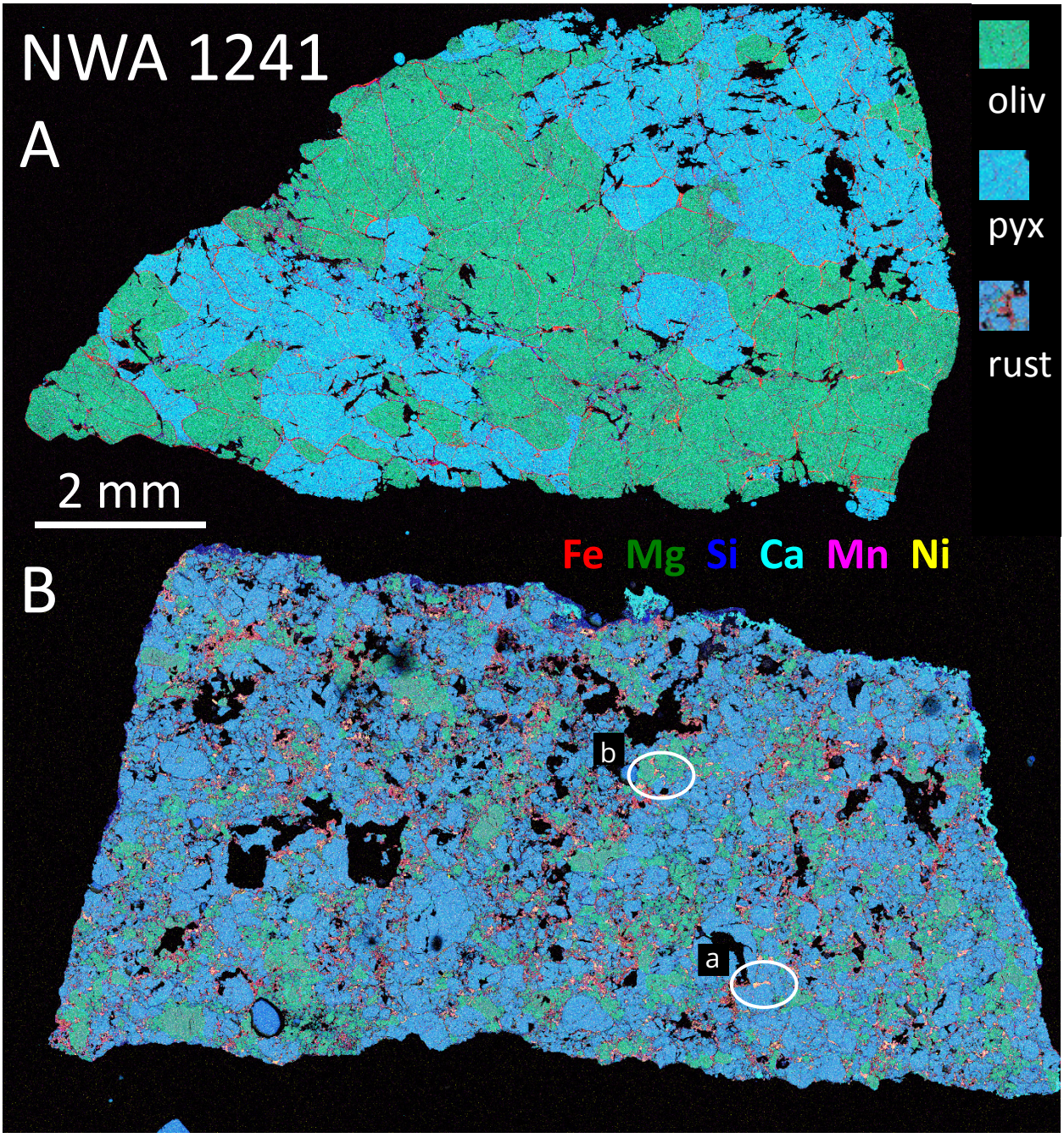
NWA 1241
A
oliv
pyx
rust
2 mm
B
Fe Mg Si Ca Mn Ni
b
a

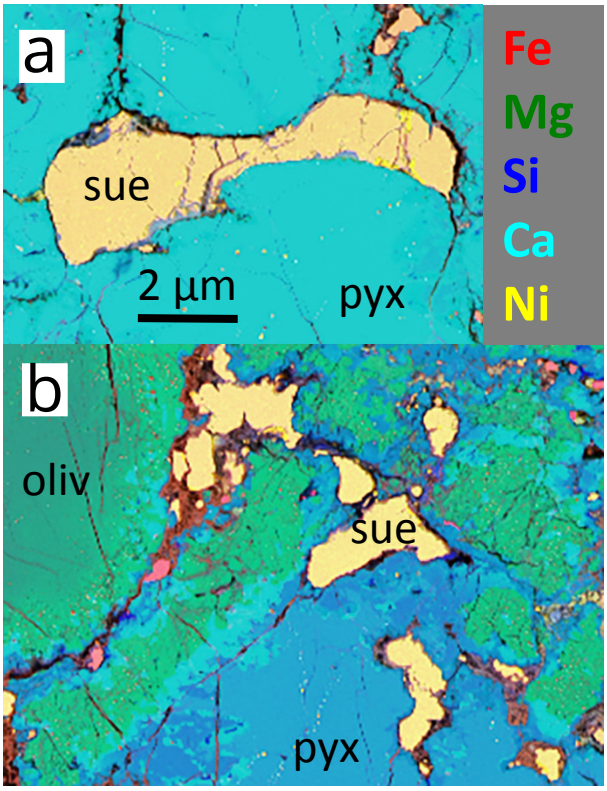
a
sue
2 µm
pyx
Fe
Mg
Si
Ca
Ni
b
oliv
sue
pyx

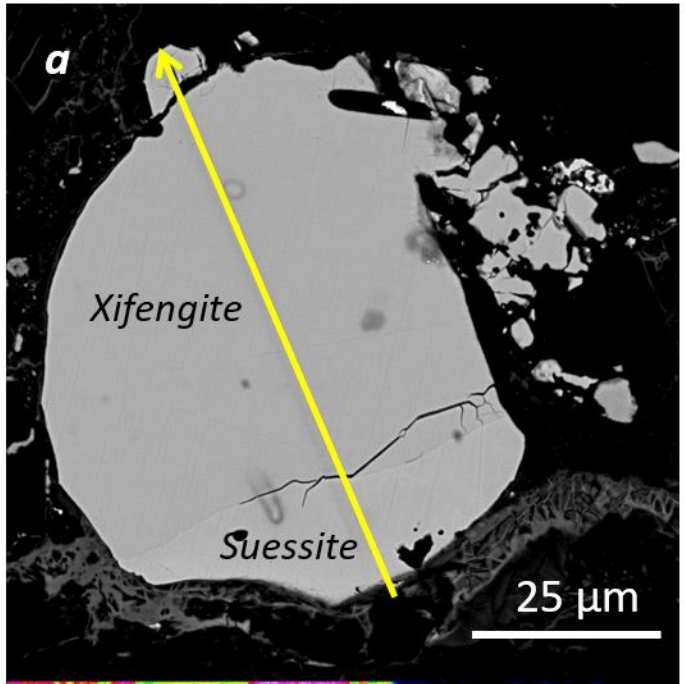
a
Xifengite
Suessite
25 µm

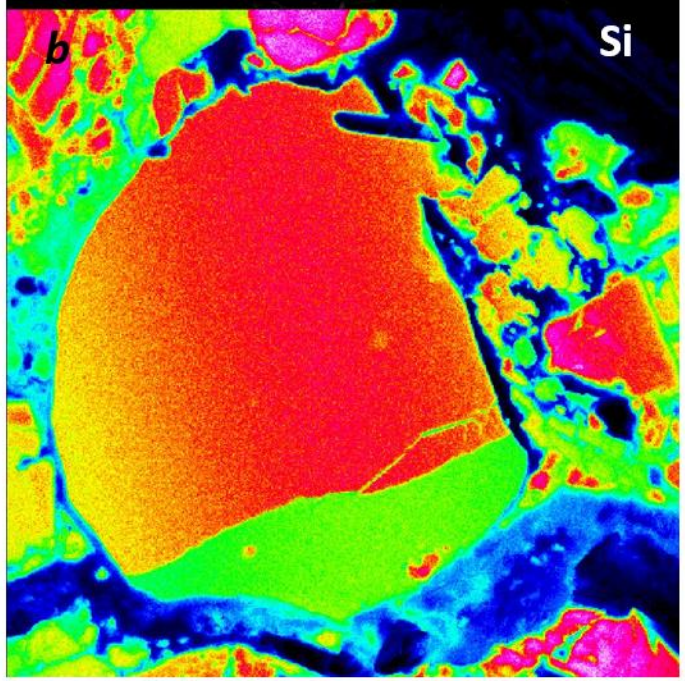
b
Si

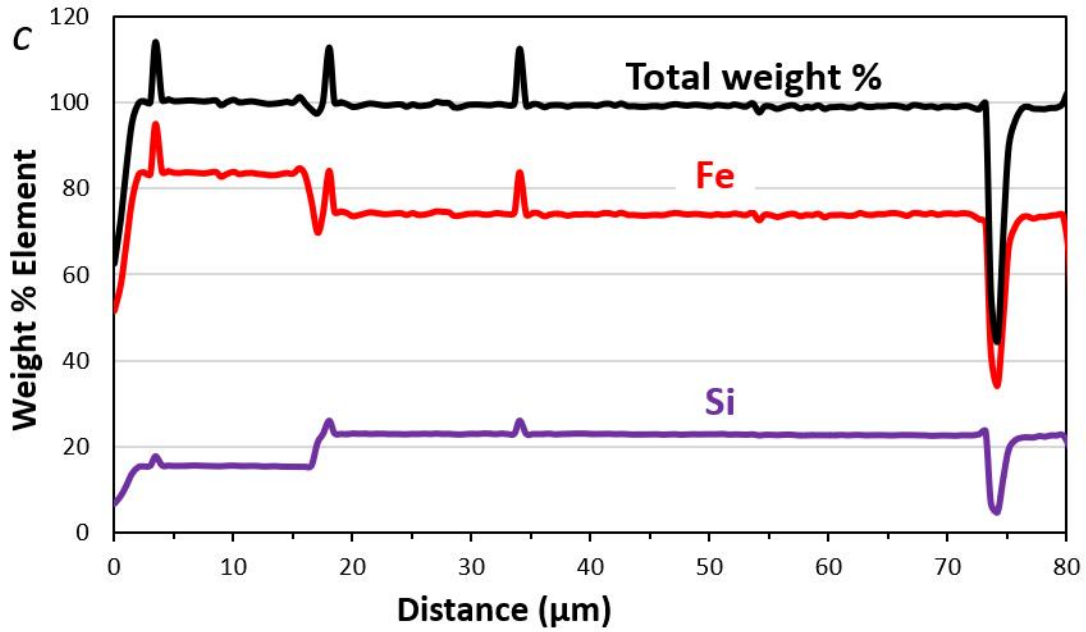
c
Total weight %
Fe
Si
Weight % Element
Distance (µm)
0
20
40
60
80
100
120
0
10
20
30
40
50
60
70
80

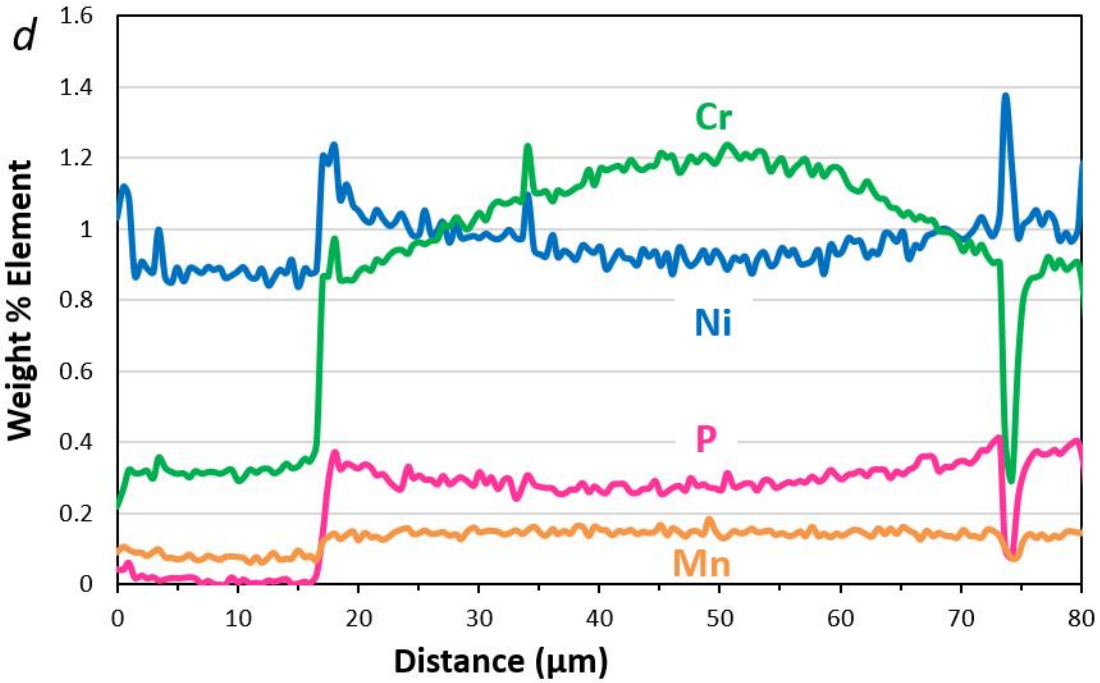
d
Cr
Ni
P
Mn
Weight % Element
Distance (µm)
0
0.2
0.4
0.6
0.8
1
1.2
1.4
1.6
0
10
20
30
40
50
60
70
80

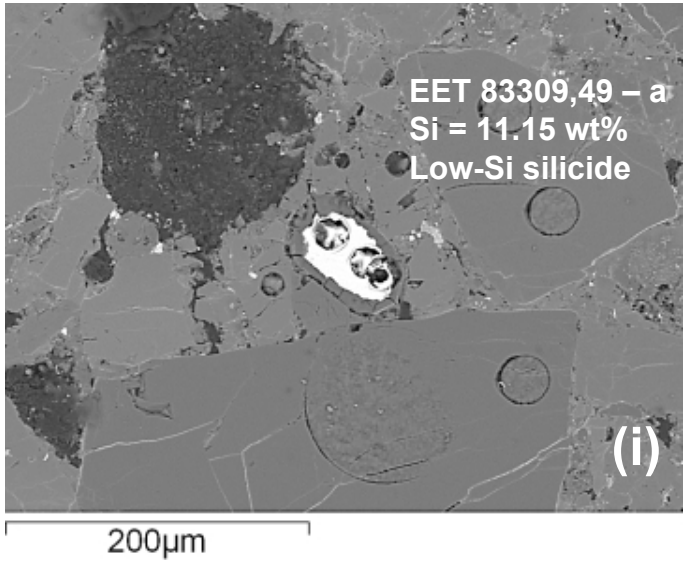
EET 83309,49 – a
Si = 11.15 wt%
Low-Si silicide
(i)
200µm

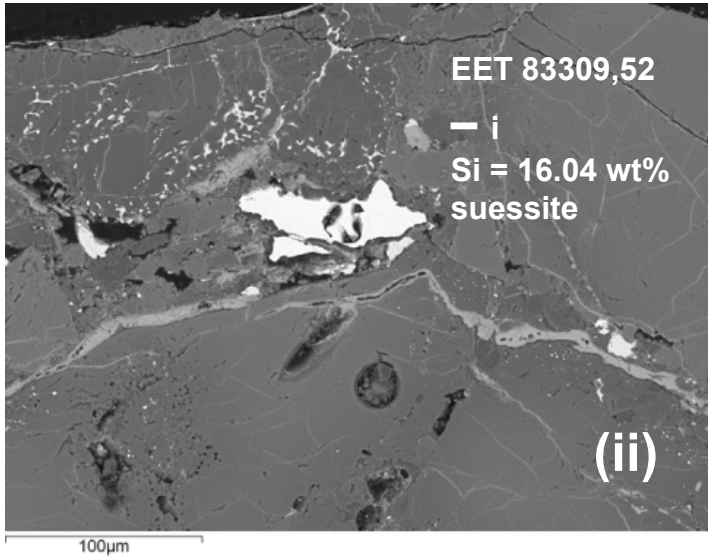
EET 83309,52
– i
Si = 16.04 wt%
suessite
(ii)
100µm

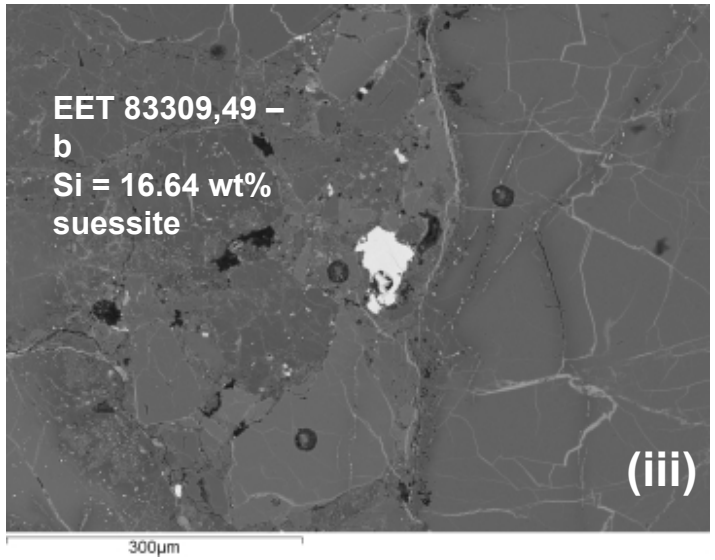
EET 83309,49 –
b
Si = 16.64 wt%
suessite
(iii)
300µm

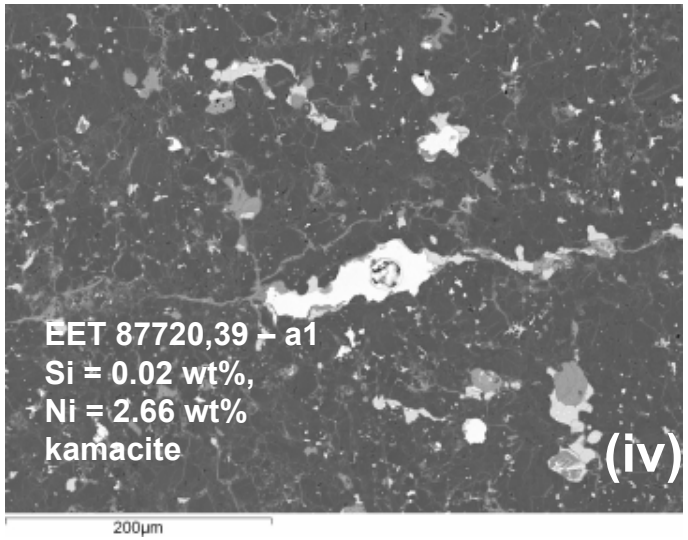
EET 87720,39 – a1
Si = 0.02 wt%,
Ni = 2.66 wt%
kamacite
(iv)
200µm

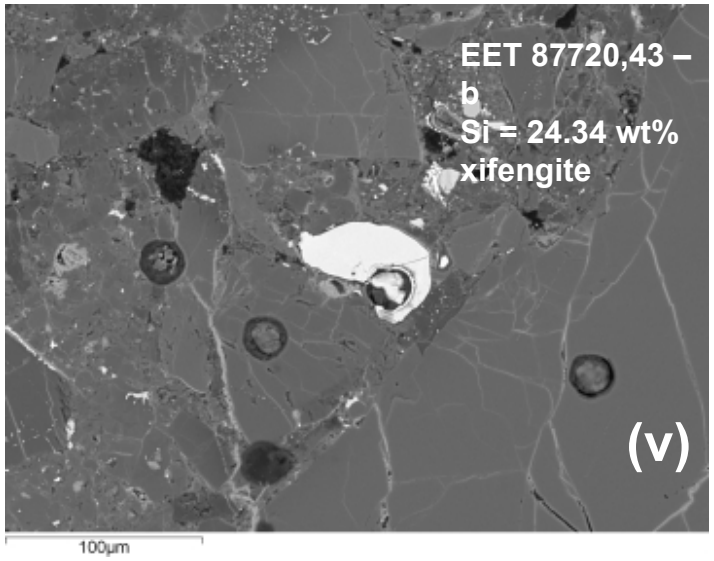
EET 87720,43 –
b
Si = 24.34 wt%
xifengite
(v)
100µm

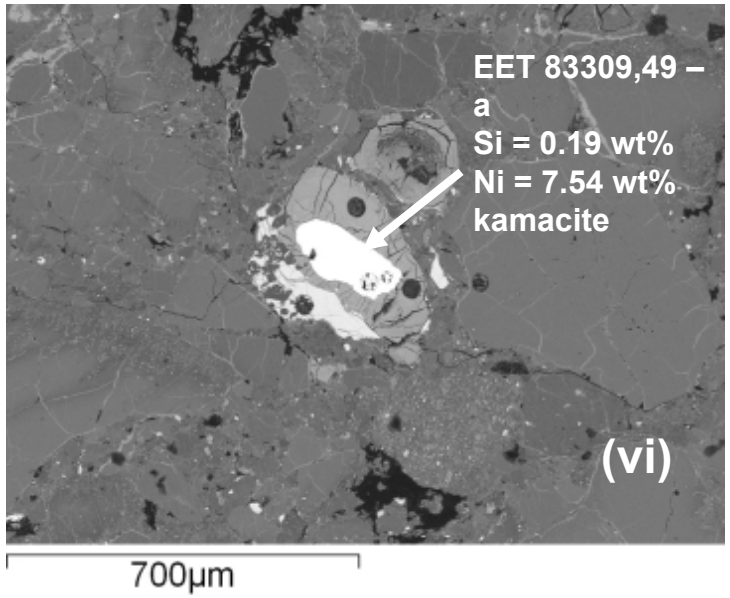
EET 83309,49 –
a
Si = 0.19 wt%
Ni = 7.54 wt%
kamacite
(vi)
700µm

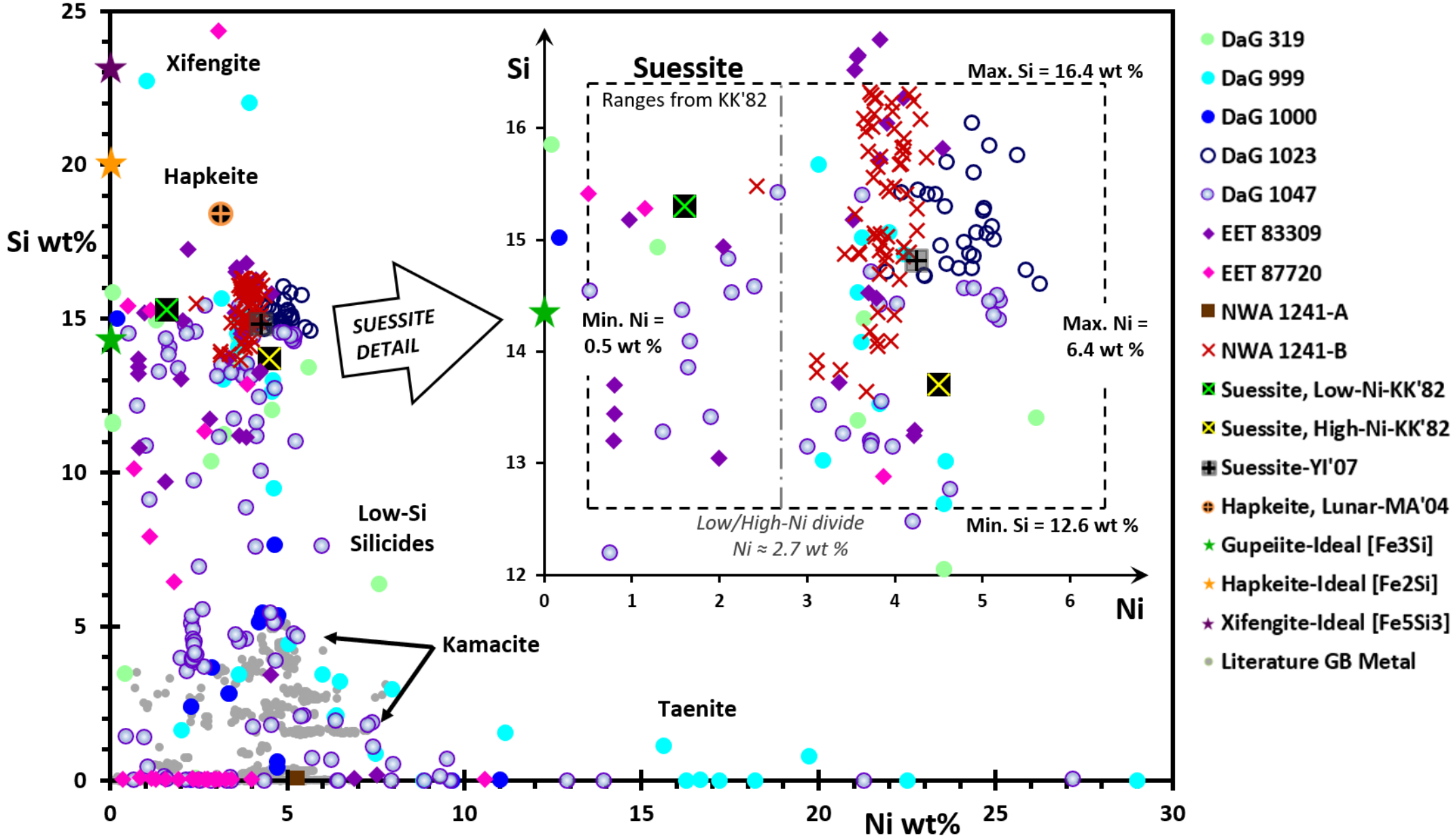
Xifengite
Hapkeite
Si wt%
Low-Si
Silicides
Kamacite
Taenite
Ni wt%
SUESSITE
DETAIL
Suessite
Ranges from KK'82
Si
Ni
Max. Si = 16.4 wt %
Min. Ni =
0.5 wt %
Max. Ni =
6.4 wt %
Min. Si = 12.6 wt %
Low/High-Ni divide
Ni ≈ 2.7 wt %
DaG 319
DaG 999
DaG 1000
DaG 1023
DaG 1047
EET 83309
EET 87720
NWA 1241-A
NWA 1241-B
Suessite, Low-Ni-KK'82
Suessite, High-Ni-KK'82
Suessite-YI'07
Hapkeite, Lunar-MA'04
Gupeiite-Ideal [Fe3Si]
Hapkeite-Ideal [Fe2Si]
Xifengite-Ideal [Fe5Si3]
Literature GB Metal

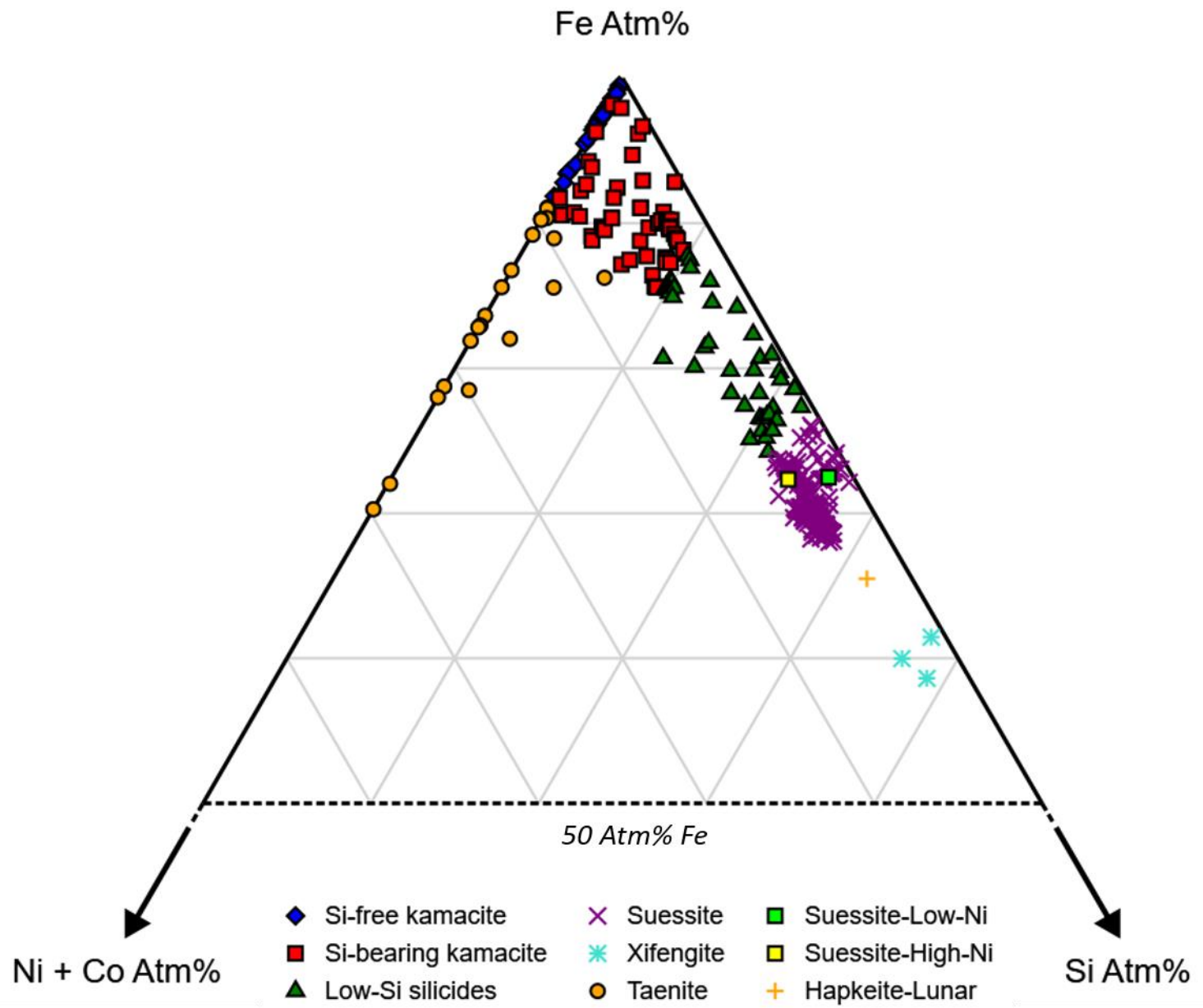
Fe Atm%
50 Atm% Fe
Ni + Co Atm%
Si Atm%
Si-free kamacite
Si-bearing kamacite
Low-Si silicides
Suessite
Xifengite
Taenite
Suessite-Low-Ni
Suessite-High-Ni
Hapkeite-Lunar

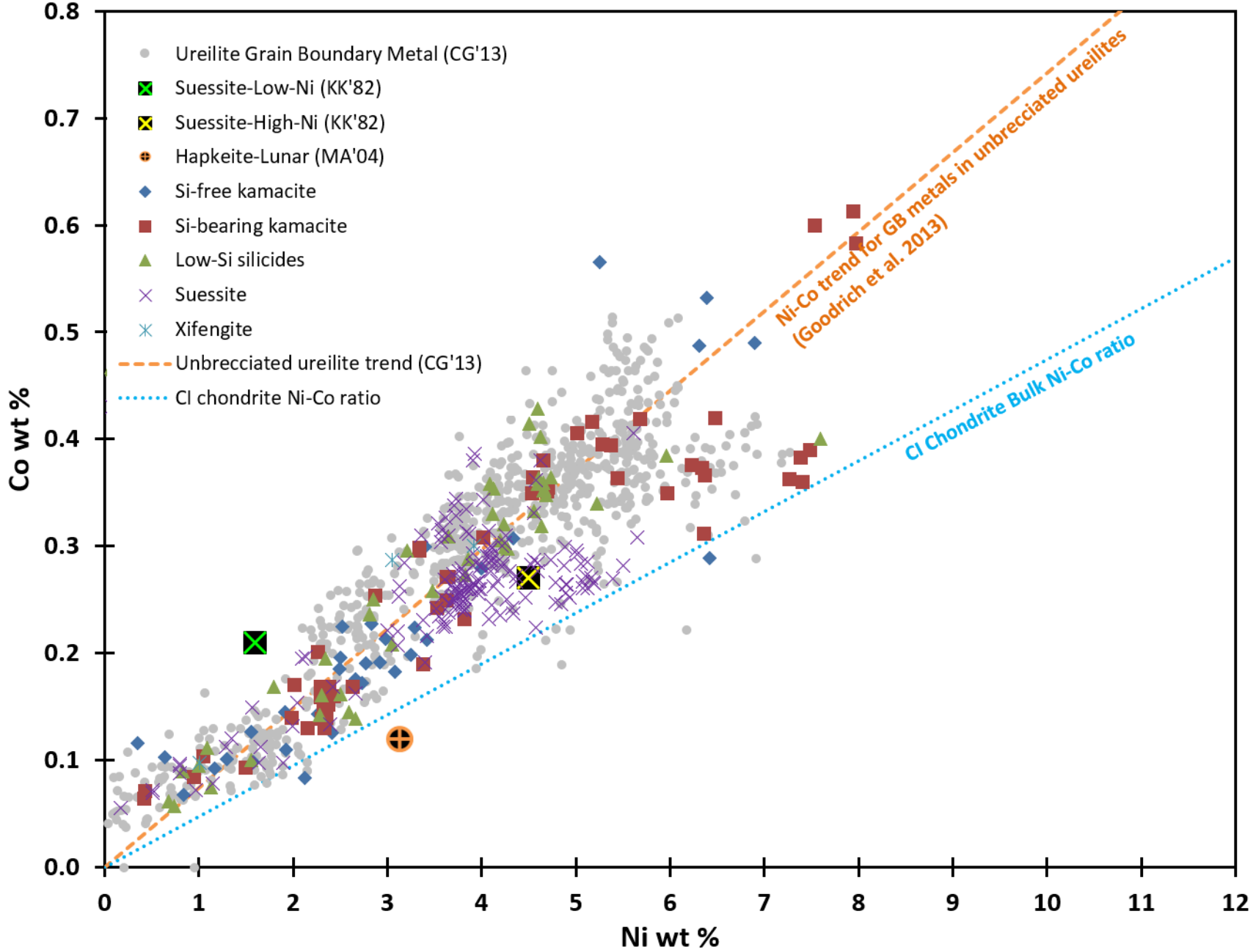
Ureilite Grain Boundary Metal (CG'13)
Suessite-Low-Ni (KK'82)
Suessite-High-Ni (KK'82)
Hapkeite-Lunar (MA'04)
Si-free kamacite
Si-bearing kamacite
Low-Si silicides
Suessite
Xifengite
Unbrecciated ureilite trend (CG'13)
CI chondrite Ni-Co ratio
Ni-Co trend for GB metals in unbrecciated ureilites (Goodrich et al. 2013)
CI Chondrite Bulk Ni-Co ratio
Co wt %
Ni wt %
0.0
0.1
0.2
0.3
0.4
0.5
0.6
0.7
0.8
0
1
2
3
4
5
6
7
8
9
10
11
12

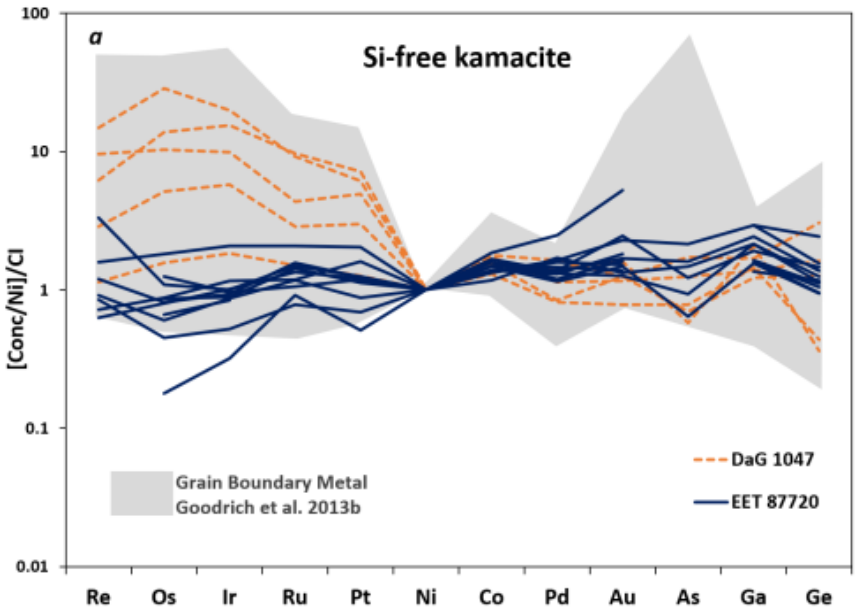
a
Si-free kamacite
[Conc/Ni]/CI
100
10
1
0.1
0.01
Re Os Ir Ru Pt Ni Co Pd Au As Ga Ge
Grain Boundary Metal
Goodrich et al. 2013b
DaG 1047
EET 87720

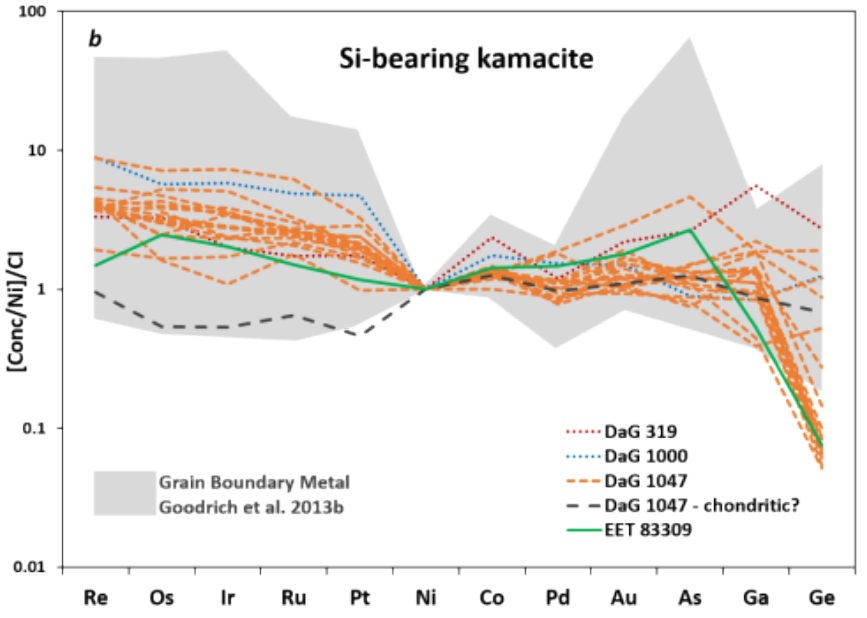
b
Si-bearing kamacite
[Conc/Ni]/CI
100
10
1
0.1
0.01
Re Os Ir Ru Pt Ni Co Pd Au As Ga Ge
Grain Boundary Metal
Goodrich et al. 2013b
DaG 319
DaG 1000
DaG 1047
DaG 1047 - chondritic?
EET 83309

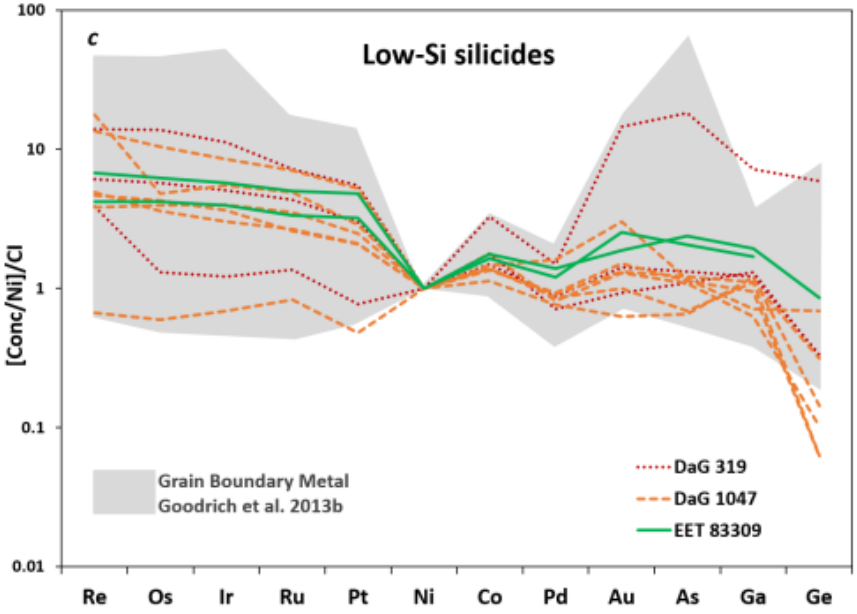
c
Low-Si silicides
[Conc/Ni]/CI
100
10
1
0.1
0.01
Re Os Ir Ru Pt Ni Co Pd Au As Ga Ge
Grain Boundary Metal
Goodrich et al. 2013b
DaG 319
DaG 1047
EET 83309

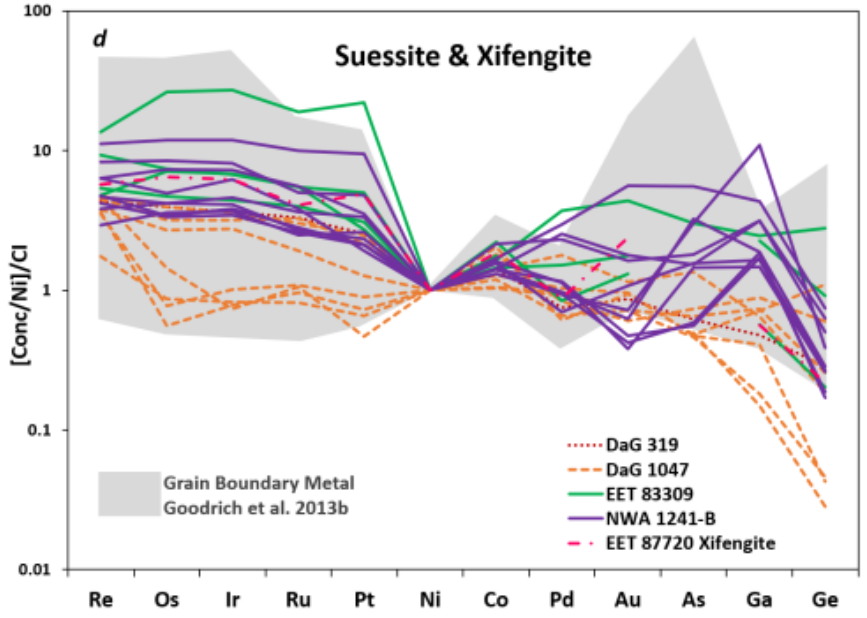
d
Suessite & Xifengite
[Conc/Ni]/CI
100
10
1
0.1
0.01
Re Os Ir Ru Pt Ni Co Pd Au As Ga Ge
Grain Boundary Metal
Goodrich et al. 2013b
DaG 319
DaG 1047
EET 83309
NWA 1241-B
EET 87720 Xifengite

Table 1. Representative major element compositions of metals in brecciated ureilites and NWA 1241-B.

SAMPLE	Si wt%	P wt%	Cr wt%	Mn wt%	Fe wt %	Co wt%	Ni wt%	S wt%	Total wt%
Si-free kamacite									
EET 87720	0.03	0.15	0.06	*na*	98.02	0.12	0.34	*bdl*	98.72
EET 87720	0.03	0.17	0.05	*na*	97.23	0.15	1.92	*bdl*	99.54
DaG 1000	*bdl*	0.11	0.09	*bdl*	95.94	0.14	2.26	*bdl*	98.55
DaG 319	0.06	0.07	0.10	*bdl*	96.83	0.13	2.41	*bdl*	99.59
EET 87720	0.03	0.20	0.12	*na*	96.33	0.19	2.49	*bdl*	99.35
DaG 1047	*bdl*	0.29	0.12	*bdl*	96.42	0.22	2.52	*bdl*	99.57
EET 87720	*bdl*	0.19	0.06	*na*	96.34	0.21	2.98	*bdl*	99.78
DaG 1047	*bdl*	0.06	0.04	*bdl*	96.77	0.22	3.29	*bdl*	100.38
DaG 1047	*bdl*	0.40	0.05	*bdl*	93.67	0.31	4.34	*bdl*	98.77
DaG 999	*bdl*	*bdl*	*bdl*	*bdl*	92.81	0.49	6.31	*bdl*	99.61
DaG 1047	*bdl*	0.04	0.07	*bdl*	93.12	0.53	6.39	*bdl*	100.14
EET 83309	0.05	*bdl*	0.05	*na*	91.87	0.49	6.89	*bdl*	99.36
Si-bearing kamacite									
EET 83309	0.19	0.45	*bdl*	*na*	90.11	7.54	0.60	*bdl*	98.89
DaG 1047	0.47	0.36	0.07	*bdl*	96.93	1.05	0.10	*bdl*	98.98
DaG 1047	0.75	0.56	0.04	*bdl*	92.24	5.68	0.42	*bdl*	99.69
DaG 999	0.87	0.15	bdl	*bdl*	90.35	7.49	0.39	*bdl*	99.25
DaG 1047	1.44	0.28	0.16	*bdl*	96.85	0.42	0.06	*bdl*	99.21
DaG 1047	1.76	0.32	0.06	*bdl*	93.41	4.02	0.31	*bdl*	99.88
DaG 1047	1.82	0.37	0.21	*bdl*	92.08	4.54	0.35	*bdl*	99.37
DaG 999	2.07	0.06	*bdl*	0.04	90.94	6.33	0.37	*bdl*	99.82
DaG 1047	2.14	0.20	0.07	*bdl*	91.51	5.44	0.36	*bdl*	99.73
DaG 1000	2.42	0.28	0.39	*na*	94.02	2.26	0.20	*bdl*	99.56
DaG 1000	2.83	0.41	0.53	*na*	92.69	3.34	0.30	*bdl*	100.10
EET 83309	3.44	0.26	0.06	*na*	91.04	4.54	0.36	*bdl*	99.71
DaG 999	3.47	0.33	0.12	0.04	92.07	3.63	0.25	*bdl*	99.91
DaG 319	3.47	0.08	0.38	*bdl*	95.73	0.43	0.07	*bdl*	100.16
DaG 1000	3.69	0.32	0.25	*na*	92.66	2.87	0.25	*bdl*	100.04
DaG 1047	3.95	0.47	0.71	*bdl*	92.39	2.33	0.15	*bdl*	99.99
DaG 1047	4.11	0.98	0.82	*bdl*	91.40	2.43	0.16	*bdl*	99.90
DaG 999	4.44	0.35	0.08	*na*	88.93	5.01	0.41	*bdl*	99.21
DaG 1047	4.60	0.42	0.75	*bdl*	91.77	2.33	0.13	*bdl*	100.00
DaG 1047	4.91	0.84	0.74	*bdl*	90.19	2.31	0.16	*bdl*	99.14
Taenite									
DaG 1000	*bdl*	0.06	*bdl*	*na*	89.19	0.46	9.65	*bdl*	99.36
EET 87720	*bdl*	*bdl*	*bdl*	*na*	87.78	0.54	10.58	*bdl*	98.91
DaG 1047	*bdl*	0.18	*bdl*	*bdl*	85.18	0.77	12.90	*bdl*	99.01
DaG 999	1.13	0.59	*bdl*	*bdl*	81.36	0.76	15.61	*bdl*	99.45
DaG 999	*bdl*	*bdl*	*bdl*	*bdl*	81.28	0.70	18.19	*bdl*	100.17
DaG 1047	*bdl*	0.66	0.03	*bdl*	77.47	0.73	21.26	*bdl*	100.15
DaG 999	*bdl*	*bdl*	*bdl*	*bdl*	76.58	0.22	22.49	*bdl*	99.29
DaG 999	*bdl*	*bdl*	0.04	*na*	68.21	1.32	28.99	*bdl*	98.57

bdl = below detection limit; na = not analysed.

Table 2. Representative major element compositions of silicides in brecciated ureilites and NWA 1241-B.

SAMPLE	Si wt%	P wt%	Cr wt%	Mn wt%	Fe wt %	Co wt%	Ni wt%	S wt%	Total wt%
Low-Si silicides									
DaG 1000	5.26	0.34	0.04	*na*	89.29	0.35	4.65	*bdl*	99.94
DaG 1000	5.45	0.24	0.07	*na*	89.86	0.30	4.27	*bdl*	100.19
DaG 319	6.38	0.24	*bdl*	*bdl*	84.85	0.40	7.60	*bdl*	99.50
EET 87720	6.46	0.46	0.72	*na*	90.48	0.17	1.79	*bdl*	100.09
DaG 1047	6.97	0.04	0.15	*bdl*	89.59	0.16	2.50	*bdl*	99.41
DaG 1047	7.64	0.26	0.06	*bdl*	85.41	0.38	5.96	*bdl*	99.71
DaG 1047	8.88	0.37	0.40	*bdl*	85.38	0.27	3.83	*bdl*	99.14
DaG 999	9.49	0.34	0.13	*bdl*	85.22	0.43	4.59	*bdl*	100.20
EET 83309	9.71	0.29	1.11	*na*	87.40	0.10	1.56	*bdl*	100.16
DaG 1047	9.77	0.40	0.37	*bdl*	86.55	0.20	2.35	*bdl*	99.63
EET 87720	10.13	0.12	0.46	*na*	88.49	0.06	0.68	*bdl*	99.95
EET 83309	10.82	0.24	0.30	*na*	88.08	0.09	0.83	*bdl*	100.35
DaG 1047	10.90	0.15	0.65	*bdl*	86.63	0.10	1.00	*bdl*	99.43
EET 87720	11.34	0.10	0.52	*na*	85.66	0.14	2.66	*bdl*	100.42
DaG 319	11.64	0.31	0.66	0.04	86.67	0.47	0.07	*bdl*	99.83
DaG 1047	11.77	0.21	0.29	*bdl*	84.01	0.26	3.48	*bdl*	100.02
Suessite									
DaG 999	12.64	0.10	0.19	*bdl*	82.69	0.33	4.56	*bdl*	100.50
DaG 1047	12.77	0.21	0.13	*bdl*	82.09	0.38	4.63	*bdl*	100.21
EET 87720	12.88	0.17	0.25	*na*	82.92	0.31	3.87	*bdl*	100.41
DaG 999	13.03	0.11	1.41	0.05	81.75	0.28	3.18	*bdl*	99.80
DaG 1047	13.17	0.10	0.77	*bdl*	81.93	0.33	3.73	*bdl*	100.01
EET 83309	13.20	0.05	0.63	*na*	86.08	0.09	0.79	*bdl*	100.85
DaG 1047	13.21	0.08	0.76	*bdl*	82.15	0.34	3.71	*bdl*	100.24
DaG 319	13.39	0.10	0.39	*bdl*	82.35	0.25	3.58	*bdl*	100.06
DaG 1047	13.42	0.09	0.35	*bdl*	84.29	0.10	1.89	*bdl*	100.14
EET 83309	13.72	0.08	0.48	*na*	81.49	0.31	3.36	*bdl*	99.44
DaG 319	14.30	0.04	0.64	*bdl*	80.95	0.31	3.65	*bdl*	99.87
DaG 1047	14.42	*bdl*	0.36	*bdl*	80.54	0.28	3.82	*bdl*	99.42
DaG 1047	14.43	0.07	1.32	0.16	79.04	0.34	4.02	*bdl*	99.38
DaG 1047	14.46	bdl	0.24	*bdl*	80.09	0.26	5.08	*bdl*	100.12
DaG 1047	14.46	0.04	0.24	*bdl*	80.12	0.27	5.19	*bdl*	100.32
EET 83309	14.48	0.11	0.09	*na*	81.92	0.28	3.79	*bdl*	100.67
DaG 1047	14.51	*bdl*	0.24	*bdl*	80.03	0.27	5.17	*bdl*	100.21
DaG 1047	14.55	*bdl*	1.23	*bdl*	82.98	0.07	0.51	*bdl*	99.34
DaG 1047	14.57	*bdl*	0.21	*bdl*	79.83	0.26	4.90	*bdl*	99.77
DaG 1023	14.61	0.20	0.05	*na*	79.86	0.31	5.65	*bdl*	100.68
NWA 1241-B	14.64	0.05	0.59	*bdl*	80.03	0.29	4.06	*bdl*	99.66
NWA 1241-B	14.69	0.04	0.76	*bdl*	80.17	0.26	3.83	*bdl*	99.75
DaG 1023	14.78	0.19	0.15	*na*	80.29	0.28	4.60	*bdl*	100.29
NWA 1241-B	14.81	0.03	0.65	*bdl*	80.29	0.26	3.89	*bdl*	99.92
DaG 1047	14.84	*bdl*	0.83	0.06	82.00	0.20	2.09	*bdl*	100.01
NWA 1241-B	14.87	0.05	0.69	*bdl*	80.11	0.26	3.90	*bdl*	99.89
DaG 1023	14.88	0.22	0.07	*na*	80.64	0.25	4.85	*bdl*	100.90
NWA 1241-B	14.89	0.04	0.58	*bdl*	80.08	0.29	4.16	*bdl*	100.04
NWA 1241-B	14.91	0.05	0.65	*bdl*	80.29	0.24	3.82	*bdl*	99.95
DaG 999	15.02	*bdl*	1.34	0.05	79.64	0.22	3.62	*bdl*	99.89
NWA 1241-B	15.03	0.04	0.74	*bdl*	79.87	0.27	3.91	*bdl*	99.85
NWA 1241-B	15.03	0.05	0.81	*bdl*	79.99	0.24	3.78	*bdl*	99.90
NWA 1241-B	15.05	0.02	0.82	*bdl*	79.97	0.26	3.84	*bdl*	99.95

DaG 999	15.07	*bdl*	0.41	*bdl*	80.37	0.39	3.93	*bdl*	100.17
NWA 1241-B	15.08	0.10	0.47	*na*	80.09	0.30	4.25	*bdl*	100.29
DaG 1023	15.12	0.08	0.17	*na*	80.01	0.27	5.10	*bdl*	100.76
EET 83309	15.18	0.06	0.38	*na*	80.94	0.24	3.52	*bdl*	100.32
NWA 1241-B	15.23	0.02	0.95	*bdl*	79.66	0.23	3.55	*bdl*	99.64
EET 87720	15.28	0.04	0.39	*na*	84.48	0.08	1.15	*bdl*	101.41
DaG 1047	15.43	*bdl*	1.46	*bdl*	80.06	0.16	2.66	*bdl*	99.77
NWA 1241-B	15.46	0.07	0.58	*na*	79.94	0.28	3.90	*bdl*	100.24
NWA 1241-B	15.48	0.08	0.69	*na*	81.81	0.17	2.42	*bdl*	100.65
NWA 1241-B	15.56	0.08	0.47	*na*	79.74	0.28	3.76	*bdl*	99.88
DaG 1023	15.61	0.07	0.28	*na*	79.58	0.26	4.90	*bdl*	100.70
DaG 999	15.68	*bdl*	1.09	0.04	80.14	0.25	3.12	*bdl*	100.33
DaG 1023	15.70	0.08	0.19	*na*	79.28	0.28	4.59	*bdl*	100.12
EET 83309	15.82	0.14	0.58	*na*	77.71	0.29	4.55	*bdl*	99.08
DaG 319	15.85	0.34	0.62	*bdl*	82.88	0.43	0.08	*bdl*	100.20
NWA 1241-B	16.00	0.06	0.67	*na*	79.31	0.28	3.99	*bdl*	100.30
NWA 1241-B	16.08	0.05	0.71	*na*	79.10	0.28	4.30	*bdl*	100.51
NWA 1241-B	16.30	*bdl*	0.73	*na*	78.92	0.26	3.74	*bdl*	99.95
NWA 1241-B	16.31	*bdl*	0.87	*na*	77.92	0.27	4.17	*bdl*	99.53
NWA 1241-B	16.32	*bdl*	0.96	*na*	79.30	0.25	3.72	*bdl*	100.55
Xifengite									
DaG 999	22.74	0.28	1.22	0.16	73.77	1.01	0.10	*bdl*	99.27
DaG 999	22.04	0.81	0.89	*na*	71.72	3.91	0.30	*bdl*	99.68

bdl = below detection limit; na = not analysed.